AD-A173 239 EFFICIENT FINITE ELEMENT METHODS FOR TRANSIENT ANALYSIS 1/1
OF SHELLS(U) NORTHWESTERN UNIV EVANSTON IL DEPT OF
CIVIL ENGINEERING T BELYTSCHKO APR 85 AFOSR-TR-86-1009
UNCLASSIFIED F49620-82-K-0013 F/G 13/13 NL

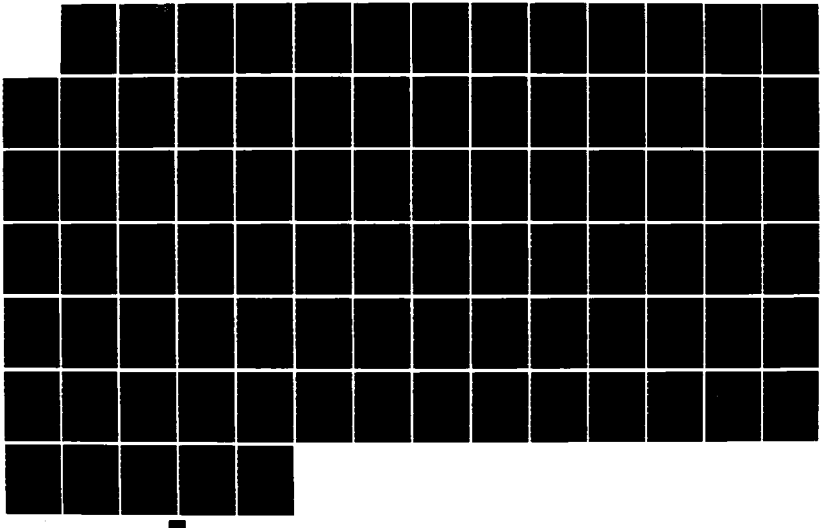

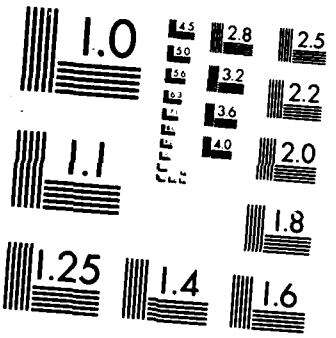

SECURITY CLASSIFI

AD-A173 239

DTIC ELECTE OCT 20 1986 S D

B

MENTATION PAGE

1a. REPORT SECURITY CLASSIFICATION UNCLASSIFIED	1b. RESTRICTIVE MARKINGS
2a. SECURITY CLASSIFICATION AUTHORITY	3. DISTRIBUTION/AVAILABILITY OF REPORT Approved for public release, distribution unlimited
2b. DECLASSIFICATION/DOWNGRADING SCHEDULE	
4. PERFORMING ORGANIZATION REPORT NUMBER(S)	5. MONITORING ORGANIZATION REPORT NUMBER(S) AFOSR-TR- 86-1009
6a. NAME OF PERFORMING ORGANIZATION Northwestern University 6b. OFFICE SYMBOL (If applicable)	7a. NAME OF MONITORING ORGANIZATION Air Force Office of Scientific Research
6c. ADDRESS (City, State and ZIP Code) Department of Civil Engineering Evanston, IL 60201	7b. ADDRESS (City, State and ZIP Code) Bolling Air Force Base, DC 20332-6448
8a. NAME OF FUNDING/SPONSORING ORGANIZATION Air Force Office of Sci. Res. 8b. OFFICE SYMBOL (If applicable) NA	9. PROCUREMENT INSTRUMENT IDENTIFICATION NUMBER F49620-82-K-0013
8c. ADDRESS (City, State and ZIP Code) Air Force Office of Scientific Research Bolling Air Force Base, DC 20332-6448	10. SOURCE OF FUNDING NOS. PROGRAM ELEMENT NO.: 61102F PROJECT NO.: 2302 TASK NO.: B1 WORK UNIT NO.:
11. TITLE (Include Security Classification) Efficient Finite Element Methods for Transient Analysis of Shells	
12. PERSONAL AUTHOR(S) T. Belytschko	
13a. TYPE OF REPORT Final 13b. TIME COVERED FROM Feb. 81 TO Feb. 84	14. DATE OF REPORT (Yr., Mo., Day) April 1985 15. PAGE COUNT 81
16. SUPPLEMENTARY NOTATION	

17. COSATI CODES			18. SUBJECT TERMS (Continue on reverse if necessary and identify by block number)
FIELD	GROUP	SUB. GR.	
			Finite elements, shells, structural dynamics, kinematic modes, hourglass control, reduced integration

19. ABSTRACT (Continue on reverse if necessary and identify by block number)

Efficient and accurate elements for the large displacement, transient analysis of shells have been developed. The essential feature of these elements is the use of minimal quadrature, which consists of 1 point quadrature in the 4-node quadrilateral or the 3-node triangle, and 2x2 quadrature in the 9-node element. Since these minimal quadrature elements possess spurious singular modes, their use requires effective control of these modes. A control procedure has been developed which satisfies consistency and hence does not impair the convergence of the element. This is achieved through a special γ-projection which is orthogonal to linear fields, hence these elements are called γ-elements.

In addition to these developments, the following was achieved in this project: (1) the identification of the membrane locking phenomenon which impedes the convergence of any fully integrated curved element; (2) the development of general methods for (cont.)

20. DISTRIBUTION/AVAILABILITY OF ABSTRACT UNCLASSIFIED/UNLIMITED ☐ SAME AS RPT. ☐ DTIC USERS ☐	21. ABSTRACT SECURITY CLASSIFICATION Unclassified
22a. NAME OF RESPONSIBLE INDIVIDUAL Dr Anthony Amos	22b. TELEPHONE NUMBER (Include Area Code) (202) 767-4953 22c. OFFICE SYMBOL AFOSR-NA

DD FORM 1473, 83 APR EDITION OF 1 JAN 73 IS OBSOLETE

19. Abstract: (Continued)

ameliorating membrane locking through both explicit mode decomposition projections and through implicit projections by means of reduced integration; (3) the development of stabilization procedures for higher order elements such as the 9-node element which satisfy basic consistency and the patch test.

PREFACE

The work described in this report was conducted in the Department of Civil Engineering at Northwestern University under the direction of Professor Ted Belytschko. The following technical personnel participated in this research: Wing-Kam Liu, Henryk Stolarski, N. Carpenter and J.S. Ong. N. Carpenter and J.S. Ong will be receiving their Ph.D. degrees in 1985. The Air Force program monitor was Dr. Anthony Amos.

AFOSR-TR- 86-1009

The results of this work have appeared in the following journal papers:

H. Stolarski, T. Belytschko and N. Carpenter, "Bending and Shear Mode Decomposition in C^0 Structural Elements," J. of Structural Mechanics, 11(2), 153-176, 1983.

H. Stolarski and T. Belytschko, "Shear and Membrane Locking in Curved C^0 Elements," Computer Methods in Applied Mechanics and Engineering, 14, 279-296, 1983.

T. Belytschko, J.I. Lin and C.S. Tsay, "Explicit Algorithms for the Nonlinear Dynamics of Shells," Computer Methods in Applied Mechanics and Engineering, 42, 225-251, 1984.

T. Belytschko, H. Stolarski and N. Carpenter, "A C^0 Triangular Plate Element with One-Point Quadrature," Intl. J. Num. Methods in Eng., 20(5), 787-802, 1984.

T. Belytschko, J.S.-J. Ong, W.K. Liu and J.M. Kennedy, "Hourglass Control in Linear and Nonlinear Problems," Computer Methods in Appl. Mechanics and Engineering, 43, 251-276, 1984.

T. Belytschko, J.S.-J. Ong and W.K. Liu, "A Consistent Control of Spurious Singular Modes in the 9-Node Lagrange Element for the Laplace and Mindlin Plate Equations," Comp. Meth. in Appl. Mech. and Engrg., 44, 269-295, 1984.

H. Stolarski, T. Belytschko and N. Carpenter, "A Simple Triangular Curved Shell Element," Engineering Computations, 1, 210-218, 1984.

The following papers are in review or in press:

T. Belytschko, H. Stolarki, W.K. Liu, N. Carpenter and J.S.-J. Ong, "Stress Projection for Membrane and Shear Locking in Shell Finite Elements," in press Computer Methods for Applied Mechanics and Engineering.

H. Stolarski and T. Belytschko, "On the Equivalence of Mode Decomposition and Mixed Finite Elements," to appear Computer Methods for Applied Mechanics and Engineering.

N. Carpenter, H. Stolarski and T. Belytschko, "A Flat Triangular Shell Element with Improved Membrane Interpolation," Communications in Applied Numerical Methods, in press 1985.

Results of this work were presented at the following meetings:

"Hourglass Control for Linear and Nonlinear Problems," ASME Applied Mechanics Division Summer Annual Meeting, Houston, Texas, June 21, 1983, (with W.K. Liu, J.S.J. Ong, J.M. Kennedy)

"Nine-Node Lagrange Shell Elements with Spurious Mode Control," Proc. AIAA/ASME/Structural Dynamics Conference Palm Springs, CA, May 1984 (with W.K. Liu, J.S.J. Ong)

"Implementation and Application of a 9-Node Lagrange Shell Element with Spurious Mode Control," Symposium on Advances and Trends in Structures and Dynamics, Washington, D.C., Oct. 1984 (with W.K. Liu, J.S.J. One, D. Lam)

Invited lecture: "Stress Projection for Membrane and Shear Locking in Shell Finite Elements," FENOMECH Conference, Institut fur Statik & Dynamik, Stuttgart, Germany, Sept. 1984 (with H. Stolarski, W.K. Liu, N. Carpenter, J.S.J. Ong)

"Test Problems for Shell Finite Elements," AIAA/ASME/ASCE/AHS 26th Structures, Structural Dynamics and Materials Conference, Orlando, Florida, April 1985 (with W.K. Liu).

"A Simple Triangular Curved Shell Element for Collapse Analysis," ASME Pressure Vessel & Piping Conference, San Antonio, Texas, June 1984.

INTRODUCTION

The purpose of this research was to develop efficient and accurate finite elements for the large displacement, transient analysis of shells. It was apparent from the beginning of this research program that in order to achieve these goals, minimal quadrature rules would have to be developed so that the fewest possible number of quadrature points would be used in an element. In the case of the 4-node shell element, minimal quadrature consists a single quadrature point per element; in the 9-node Lagrange shell element, minimal quadrature is a 2x2 Gauss quadrature. Compared to full quadrature, reduced quadrature reduces solution time by 50% to 75% and also enhances the accuracy of shell elements.

However, minimal quadrature elements have one important shortcoming: they possess spurious singular modes, often known as hourglass modes, which can completely destroy a solution. Therefore, procedures were developed for controlling these spurious modes. These methods have been called γ-methods and they involve a special projection so that the consistency, that is the ability to meet the patch test, of the finite element is not lost. We have been able to apply these methods to both linear and nonlinear problems as evidenced by the results reported in Belytschko, Tsay and Lin (1981). Some of the nonlinear results obtained in that paper are reviewed in Appendix C of this report. It can be seen from these results, that the method has indeed become effective in providing accurate nonlinear solutions. The method has already been incorporated in the general purpose program ABAQUS.

In addition to the basic development of the stabilization procedure, the major findings of this project are: (1) the identification of the membrane locking phenomenon which impedes the convergence of any fully integrated curved element; (2) the development of general methods for ameliorating

membrane locking through both explicit mode decomposition projections and through implicit projections by means of reduced integration; (3) the development of stabilization procedures for higher order elements such as the 9-node element which satisfy basic consistency and the patch test.

The motivation for the research into the curved elements can be understood by examining Figure 1a. These results were obtained with the widely-used, 9-node Lagrange C^0-shell element. As can be seen, it is difficult to choose a quadrature scheme for the 9-node element which is both accurate and stable. For full integration (3x3) or selective reduced integration, even a relatively fine mesh such as this results in errors which are unacceptably large. On the other hand, uniform reduced integration, which in this case is 2x2 on all terms, provides good accuracy but results in singularity of the assembled stiffness for some support conditions. This limitation of uniform reduced integration probably makes it unacceptable for general purpose programs, but its superior accuracy is attractive.

The relatively poor performance of the fully-integrated (3x3) 9-node Lagrange element in the simple arch problem is actually a mild case of misbehavior. As shown in Fig. 1b, for more complex, deeply-curved shells, the behavior of both the 3x3 and selective-reduced integration schemes can be simply abysmal. In this case, 1445 degrees of freedom for a quadrant of a shell yielded results which were only 26% of the exact solution.

A similar impasse has evolved in the development of 3-node, 18 degree-of-freedom triangular shell elements. Essentially, prior to this research no element of this genre existed which could solve a wide class of shell problems with acceptable accuracy. While certain elements performed well for specific problems, invariably when tested on a set of demanding shell test problems, their performance is unsatisfactory.

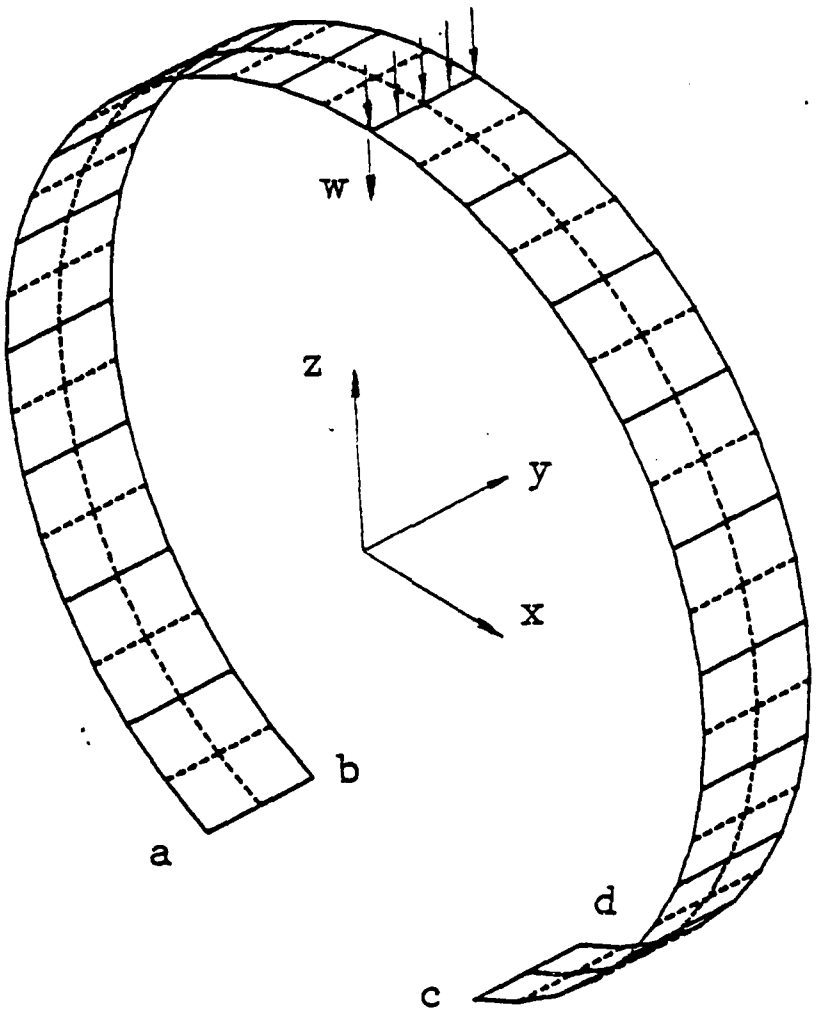

$\frac{W_{FEM}}{W_{anal}}$	clamped	pinned	6 DOF support*
full 3X3	0.702	0.760	–
S R I	0.830	0.830	0.850
reduced 2X2	1.006	1.005	fails, K is singular

*at a and d, $u_x = u_y = 0$, at b and c, $u_z = 0$

Figure 1a. Arch problem and results with various boundary conditions and quadrature schemes for 9-node Mindlin shell element.

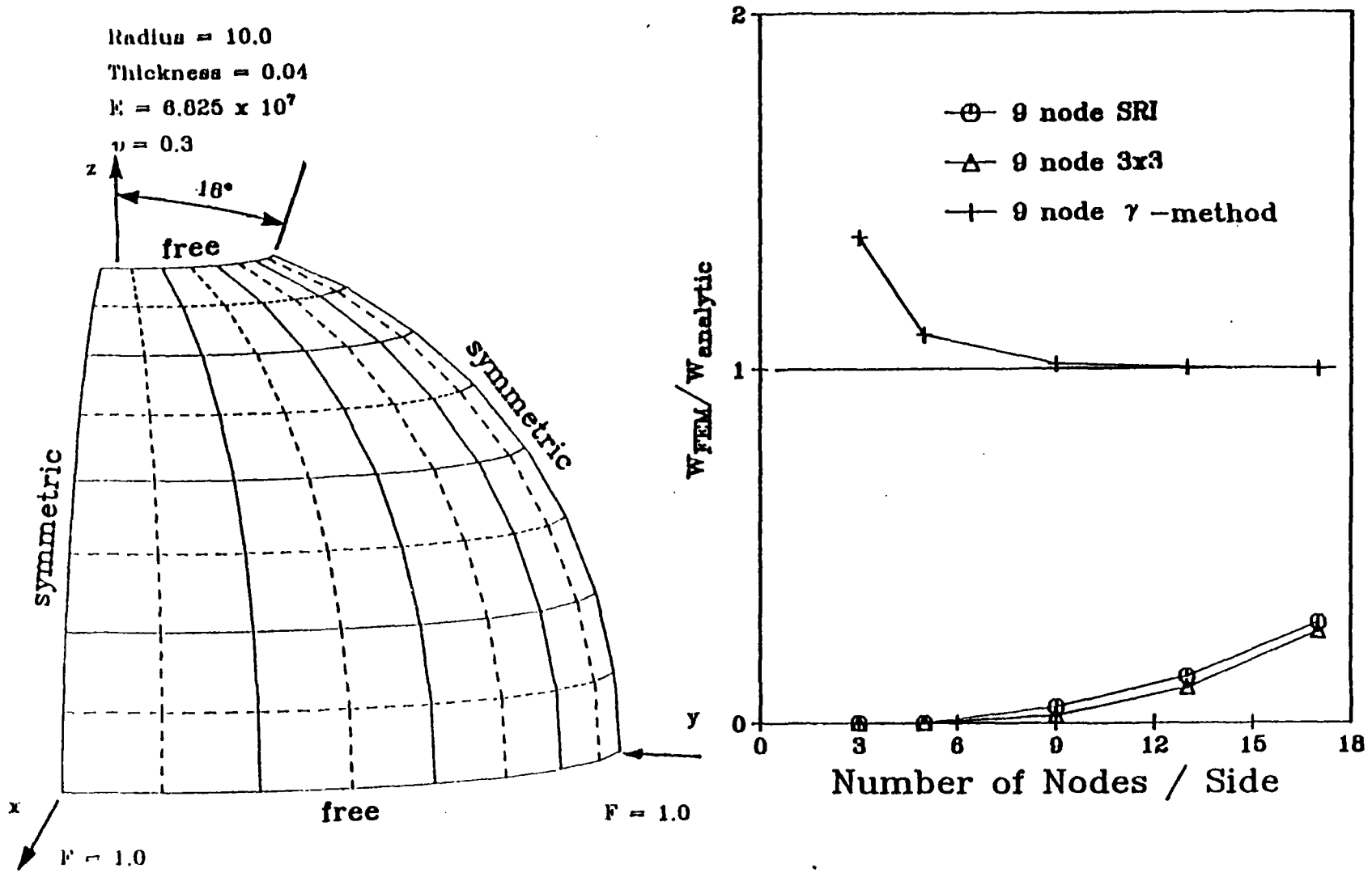

Figure 1b. Convergence of 9-node Mindlin shell element for 3x3 integration and selective reduced integration (SRI).

Two of the phenomena which have been identified as the culprits in poor element performance are shear and membrane locking. Shear locking was first identified by Doherty et al. (1969) and Ziekiewicz et al. (1971), who at the same time proposed the daring remedy of reduced integration. Reduced integration, and its offspring, selective reduced integration (SRI), proved to be very successful in ameliorating the effects of shear locking in the analysis of plates and shells.

The term "membrane locking" was coined by Stolarski and Belytschko (1981) (see also Stolarski and Belytschko (1982)), who showed that it is related to an inadequate representation of inextensional deformation. The poor performance of many elements in analyzing the response of shells where inextensional modes of deformation are important has been noted by numerous authors, including Ashwell and Sabir (1971), Sabir and Ashwell (1971), Morley (1972), Sabir and Lock (1973), Fried (1973) and Dawe (1974). Problems related to inextensional bending were also discussed later by Ashwell (1976), Lee and Pian (1978), Noor and Peters (1981), Kikuchi (1982), Allman (1982), MacNeal (1982), Morley (1983) Stolarski and Belytschko (1983) and Kikuchi and Aizawa (1984). Reduced integration is also effective in mitigating membrane locking; see Parisch (1979) and Stolarski and Belytschko (1983).

However, prior to the work performed in this contract, membrane locking in complex shell elements was poorly understood and its pervasiveness not appreciated. Thus many users of degenerated elements did not anticipate its appearance in those elements, for the idea expressed in Noor and Peters (1981), that this locking "is a result of inadequate representation of rigid body modes" was widely held. Yet degenerated isoparametrics, which correctly incorporate rigid body motion, as first noted by Argyris and Scharpf (1968), also encounter severe membrane locking.

This contract has shown that locking can be eliminated by projection methods. Among these are mixed formulations, in which separate interpolants are used for the stresses and displacements as in Lee and Pian (1978) and Noor and Peters (1981), or by mode decomposition methods in which the nodal displacements are projected so as to minimize parasitic stresses. Examples of the latter are the Hughes and Tezduyar (1981) quadrilateral plate element and the Belytschko, et al. (1984c) triangular plate element. A common feature of all of these methods, mixed formultions, reduced integration and mode decomposition, is that they can be viewed as stress projections. Stress projections are methods in which the stresses are projected on a subspace of stresses. If the stress projection is designed so that parasitic shear stresses are reduced, then shear locking is mitigated. Similarly, stress projections that reduce parasitic membrane stresses reduce membrane locking.

The classification of projection methods as developed in this contract is summarized in Fig. 2. They are classified as (1) implicit projection methods, such as reduced integration, and (2) explicit projection methods, such as mixed methods and mode decomposition methods. Mode decomposition projections are the most explicit of these methods in that algebraic procedures are used to remove parasitic stresses. All of the projection methods ameliorate locking by annihilating parasitic shear and membrane stresses.

The outline of the report is as follows: in Section 1 a simple model will be used to show the similarity of the causes of shear and membrane locking and their relationship to parasitic shear and membrane stresses. Section 2 will then describe how mode-decomposition stress projection methods can be used to alleviate shear and membrane locking. Section 3 will show that in mode decomposition projection methods the standard B-matrix is projected onto the interpolation for the stresses. In Section 3 it is shown that the 9-

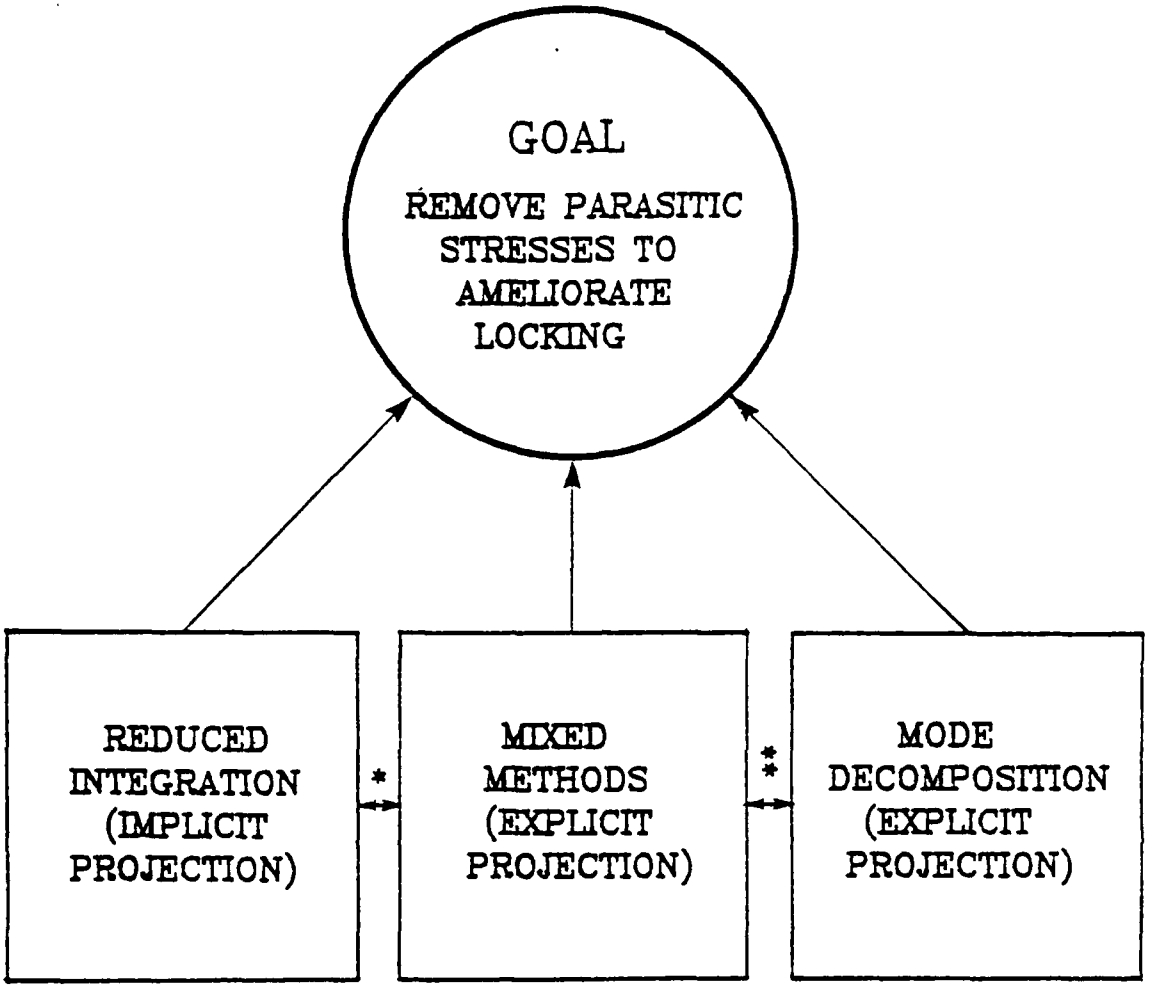

* EQUIVALENCE THEOREM OF MALKUS & HUGHES (1978)

** EQUIVALENCE THEOREM OF STOLARSKI & BELYTSCHKO (1985)

Figure 2. Schematic showing relationship of various methods of projection and the goal of eliminating locking through reduction of parasitic stresses.

node Lagrange element with 2x2 integration represents a stress projection which is free of parasitic shear and membrane stresses, and hence free of membrane and shear locking. This element is rank deficient and requires stabilization; a γ-stabilization developed in this contract is described in Appendix A. In Appendix B, a formal equivalence is established between this element and an exactly integrated mixed method.

In Section 5 a challenging set of tests problems for linear analysis of shells is desscribed. We have found these problems to be very decisive in establishing the viability of elements and have called it an obstacle course. The performance of the new elements developed here and some older elements on the obstacle course is described in Section 6. It is concluded that the 9-node element with uniform 2x2 quadrature and the γ-stabilization developed in this contract performs superbly on this set of problems.

1. SHEAR AND MEMBRANE LOCKING IN CURVED BEAMS

For purposes of examining the causes of shear and membrane locking, we will consider a curved beam described by a one dimensional version of the Marguerre shallow shell equations. Although this is one of the less popular methods for treating curved shells by finite elements, it should be stressed that the mechanical behavior of elements described by alternative methods such as degenerate shell theories and classical deep shell theories is identical as long as the shell element is shallow; the convergence of shallow shell equations expressed in Cartesian components to deep shell results has been effectively argued by Idelsohn (1981). Stolarski et al. (1985) have extended those arguments to degenerated shell theories.

In most practical applications, shell elements are quite shallow because larger elements would prevent the achievement of satisfactory accuracy. Furthermore, locking effects increase with increasing curvature. Thus the Marguerre theory provides an ideal vehicle for the study of locking in curved elements.

The kinematic relations for the Marguerre beam are given by

$$\varepsilon = u_{,x} + w^{o}_{,x} w_{,x} \tag{1.1}$$

$$\kappa = -\phi_{,x} \tag{1.2}$$

$$\gamma = w_{,x} - \phi \tag{1.3}$$

Here u and w are the x and y components of the displacement of the midline and ϕ is the rotation of the cross-section and the rigid body motion is

removed from w, so that w is the displacement relative to the chord, see Belytschko and Glaum (1979); w^o is the initial deflection of the midline from the chord of the element ε, κ and γ are the membrane strain, curvature and transverse shear strain, respectively; x is the chord of the element (see Fig. 3) and commas denote differentiation.

The stiffness matrix for an element is obtained in the displacement method by

$$f_I = \frac{\partial U}{\partial d_I} \tag{1.4}$$

where d_I is a nodal degree of freedom, f_I the corresponding nodal force and U the potential energy. For an elastic, isotropic beam the potential energy is given by

$$U = \frac{1}{2} \int_{\Omega} (D_B \kappa^2 + D_M \varepsilon^2 + D_S \gamma^2)\, d\Omega \tag{1.5}$$

where Ω is the domain of the element (length L); D_B, D_M and D_S are the bending, membrane and shear constants. For an elastic beam of thickness (depth) d and unit width, Young's modulus E and shear modulus G, these constants are given by

$$D_B = \frac{1}{12} E d^3 \tag{1.6a}$$

$$D_M = Ed \tag{1.6b}$$

$$D_S = \kappa_s G d \tag{1.6c}$$

where κ_s is the shear-correction factor. The energies associated with the constants D_B, D_M and D_S are called the bending, membrane and shear strain energies. Note that for a thin beam, d/L << 1,

$$\frac{D_B}{L^2 D_M} << 1 \qquad \frac{D_B}{L^2 D_S} << 1 \tag{1.7}$$

and the ratios of bending to membrane and bending to shear energy will similarly be small if the strains are of equal order.

Shear and membrane locking arises in curved elements because of the inability of most finite elements to achieve deformed states in which the transverse shear strain and membrane strain vanish throughout the element. Modes of deformation in which shear and membrane stresses vanish play an important role in the mechanics of shells. For example, when the moment field is constant, the transverse shear vanishes. When a shell with a single nonzero curvature, i.e. a cylindrical shell, is subjected to a state of pure bending, the membrane strains will vanish. This mode of deformation is called an inextensional mode of deformation because when the membrane strain vanishes, all lines in the middle surface of the shell remain constant in length.

In a curved finite element, inextensional states of deformation are often not possible. The consequences of this shortcoming are severe when finite elements are used to analyze a shell which undergoes inextensional bending. Because of the inequalities which hold for thin beams, (1.7), even a small membrane strain or transverse shear strain will cause the membrane or shear energy to overshadow the bending energy. Therefore, if a finite element is used to model a shell deforming in pure bending, it must be capable of representing this deformation so that only the bending energy is nonzero. Any

shear or membrane strains which are developed will absorb a substantial amount of energy and the element will behave too stiffly, which is known as locking. The stresses associated with these spurious energies are often called parasitic shear and membrane stresses. Elimination of parasitic shear and membrane stresses will eliminate locking.

It will now be shown that many of the commonly used elements will exhibit locking. Substituting Eqs. (1.1) to (1.3) into (1.5) yields

$$U = \frac{1}{2} \int_{\Omega} [D_B \phi^2_{,x} \quad + \text{ bending energy}$$
$$+ D_M (u_{,x} + w^0_{,x} w_{,x})^2 \quad + \text{ membrane energy} \qquad (1.8)$$
$$+ D_S (w_{,x} - \phi)^2] \, d\Omega \quad + \text{ shear energy}$$

If we consider a quadratic, isoparametric element, then the three displacement components and the initial displacement of the midline from the chord are given by quadratic, Lagrange shape functions N_I , so

$$[u, w^0, \phi, w] = \sum_{I=1}^{3} N_I(x) [u_I, w^0_I, \phi_I, w_I] \qquad (1.9)$$

From Eqs. (1.8) and (1.9), it can be seen that if (1) $w^0 \neq 0$ (i.e. if the shell is curved - see Fig. 3), and (2) if $w \neq 0$, then the membrane energy will be nonzero because $u_{,x}$ is linear and cannot cancel $w^0_{,x} w_{,x}$, which is quadratic. Since the two conditions of the previous sentence are met in a state of inextensional bending, this element will exhibit parasitic membrane stresses and be subject to membrane locking when the stiffness is integrated accurately; this behavior has been studied by Stolarski and Belytschko (1983). A 9-node Lagrange shell element will encounter the same difficulties.

Remark. Note that w is the transverse displacement relative to the chord, so that it vanishes in rigid body motion; otherwise, nonzero membrane strain appears in rigid body rotation.

Similarly, because ϕ is a polynomial of higher order than $w_{,x}$ in this element, it is clear from (1.8) that parasitic shear energy will appear. However, because the order of the polynomial associated with parasitic shear is lower than that associated with parasitic membrane strains, shear locking will not be as pervasive or damaging in this element as membrane locking.

Similar locking mechanisms can also be shown to occur for the cubic, isoparametric Lagrange elements, although the results of Arnold (1981) show that the locking phenomenon diminishes as the order of the polynomials increase. For linear isoparametrics, no membrane locking occurs because $w^0_{,x}$ vanishes.

In Kirchhoff or C^1 elements, only membrane locking occurs since the relation $w_{,x} = \phi$ is incorporated in the element, so that the transverse shears vanish. The membrane locking phenomenon in these elements can be quite severe. For example, in a standard beam with w^0 and w interpolated by cubic Hermite interpolants and u interpolated by linear interpolants, the term $w^0_{,x}\, w_{,x}$ is a quartic, so it cannot be effectively negated by $u_{,x}$, which is only a constant.

Some investigators have advocated using a higher order interpolation for u than w so that the membrane strain can be eliminated in pure bending modes. For example, for cubic w^0 and w, a quintic interpolant for u would enable spurious membrane strains to be suppressed. However, this remedy introduces substantial drawbacks in nonlinear analysis, for as shown by Argyris and Scharpf (1968), unless the shape functions are of the same order as that used

to represent the geometry, difficulties arise in large rotations. Rigid body motion can be adequately represented with shape functions of different order when a corotational coordinate system is used for the element, as in Belytschko and Hsieh (1973). However, the use of a single corotational system for an element with high order shape functions may introduce errors because rigid body rotation then varies substantially within a single element.

In summary, if the orders of the interpolation polynomials for u and w are such that constant moment states generate shear and membrane energy, that is parasitic stresses, then locking will result. Removal of the parasitic stresses is therefore a remedy for locking.

Remark 1.1. Elements which exhibit locking do ultimately converge. Locking does not imply the absence of convergence, but indicates the inability of the element to provide reasonable accuracy for coarse and moderate meshes.

Remark 1.2. Many alternative paradigms are available for locking. For example, Prathap and Bhashyam (1982) explain locking by the appearance of spurious constraint equations; Park and Flaggs (1984) explain locking through the appearance of unusually high frequencies in a Fourier analysis of the discrete equations. All of these approaches provide useful insights into the causes of locking, but in the setting of projection methods, the viewpoint of parasitic stresses appears most elucidating.

2. MODE DECOMPOSITION PROJECTION METHODS

The purpose of the mode-decomposition projection methods is to project the nodal displacements so that the parasitic stresses, and hence locking, are eliminated. In this Section, the application of projections to eliminate shear and membrane locking in simple beam elements will be described; the application of projection to a triangular shell element is also sketched.

The basic idea of mode decomposition projection methods is to define the bending mode component of any deformation and to ignore the membrane and shear strain energies associated with the bending modes. Thus the strain energy expression (1.5) becomes

$$U = \frac{1}{2} \int_{\Omega} [D_B \kappa^2 + D_M(\varepsilon - \varepsilon_b)^2 + D_S(\gamma - \gamma_b)^2] d\Omega \qquad (2.1)$$

where ε_b and γ_b are the membrane and shear strains in the bending mode. As can readily be seen from the above, in a constant moment state, the bending mode constitutes the total deformation so the membrane and shear energies will vanish, since in that case $\varepsilon = \varepsilon_b$ and $\gamma = \gamma_b$.

This mode decomposition is implemented by defining bending nodal displacements through a projection

$$\underset{\sim}{d}_b = \underset{\sim}{P}_b \underset{\sim}{d} \qquad (2.2)$$

so that

$$\begin{Bmatrix} \varepsilon_b \\ \gamma_b \end{Bmatrix} = \underset{\sim}{B}\, \underset{\sim}{P}_b\, \underset{\sim}{d} \tag{2.3}$$

The requirement that the bending parts of the membrane and shear strains, ε_b and γ_b, be those strains that occur in a constant moment state is not sufficient to identify the projection operator $\underset{\sim}{P}_b$, because it is only one of the bending modes. For other nodal displacements, it is also necessary to define the bending mode (or component) of the nodal displacements. Therefore a more general procedure must be developed.

Let us consider the mode decomposition procedure for shear projection in C^0 beam elements. The first step of this procedure is to define a Kirchhoff mode for any displacement field. A Kirchhoff mode is the displacement field $w^K(x)$ that would occur in a Kirchhoff beam with the curvature field given by Eq. (1.2); $w^K(x)$ is obtained by simply integrating the curvature twice and then choosing the constant of integration so that the Kirchhoff mode best fits the nodal displacements of the element.

For example, consider the 2 node, linear w, linear ϕ element in which

$$w = w_1(1 - \xi) + w_2\, \xi \tag{2.4a}$$

$$\phi = \phi_1(1 - \xi) + \phi_2\, \xi \tag{2.4b}$$

In this element, Eqs. (1.2) and (2.4b) yield the following curvature

$$\kappa = -\frac{1}{L}(\phi_2 - \phi_1) \equiv -\phi_{21}/L \tag{2.5}$$

and the Kirchhoff modes are given by

$$w^K(x) = -\frac{\phi_{21}}{2L} x^2 + a_1 x \qquad (2.6)$$

The constant a_1 is selected by

$$a_1 = \phi_1 \qquad (2.7)$$

so that the nodal rotations of the Kirchhoff mode match the total nodal rotations of the beam

$$w,_x^K(0) = \phi_1 \qquad (2.8a)$$

$$w,_x^K(L) = \phi_2 \qquad (2.8b)$$

This selection is based entirely on physical reasoning; the aim is to insure that in a constant moment state, such as shown in Fig. 3, the rotations are entirely associated with the Kirchhoff (i.e. the bending) mode, so that transverse shear energy vanishes in (2.1). It is not always possible to satisfy relations such as (2.8) (see for example the development of the triangular plate in Belytschko, et al. (1984)).

The Kirchhoff mode is then selected as the bending mode, so that the relation between the total nodal displacements and the bending nodal displacements follows from (2.6-8) and is given by

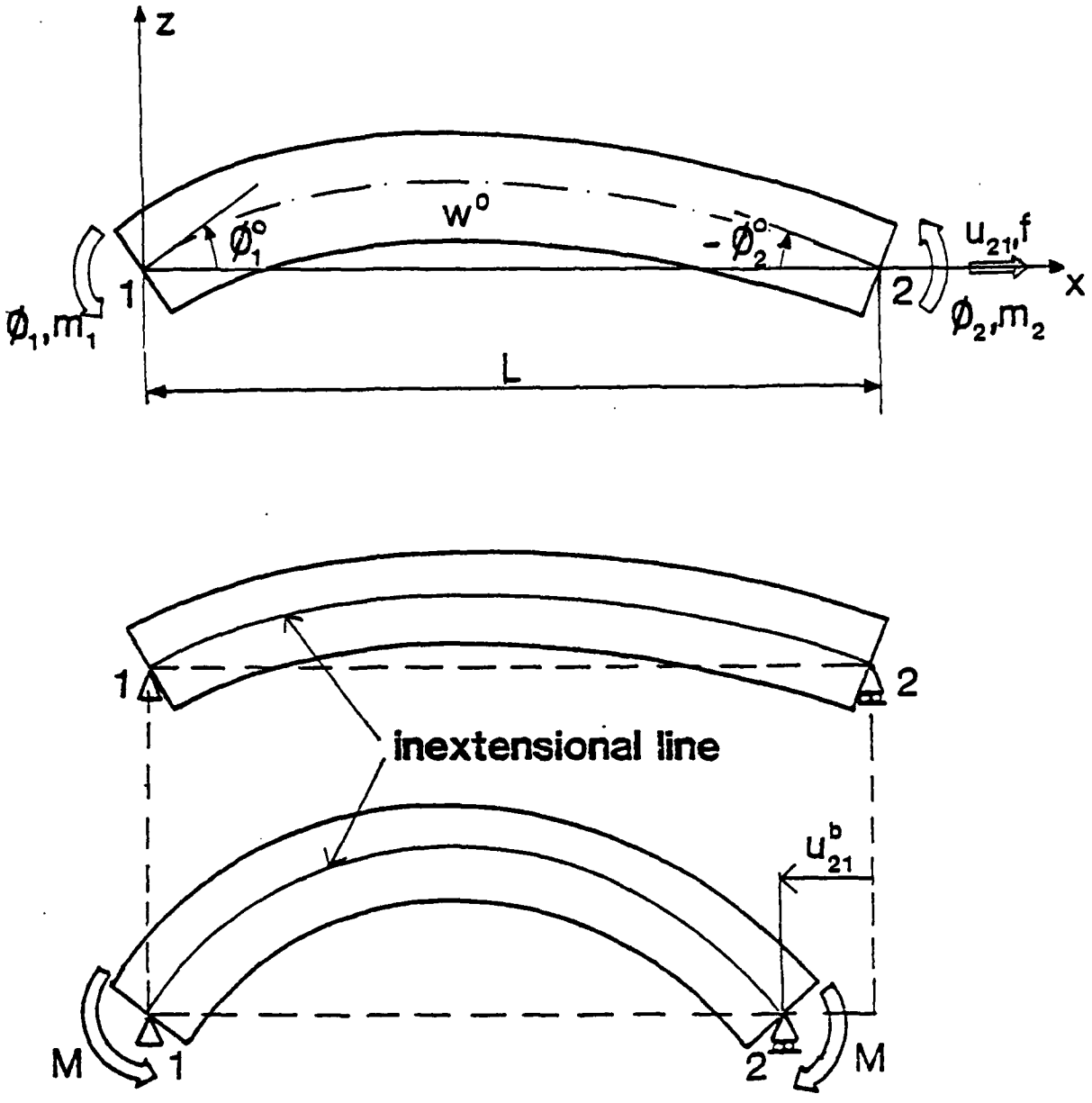

Figure 3. Nomenclature for beam element and illustration of an inextensional bending mode of deformation.

$$\begin{Bmatrix} \phi_1 \\ \phi_2 \\ w_1 \\ w_2 \end{Bmatrix}^b = \begin{bmatrix} 1 & 0 & 0 & 0 \\ 0 & 1 & 0 & 0 \\ 0 & 0 & 0 & 0 \\ L/2 & L/2 & 0 & 0 \end{bmatrix} \begin{Bmatrix} \phi_1 \\ \phi_2 \\ w_1 \\ w_2 \end{Bmatrix} \equiv \underset{\sim}{P}_b \, \underset{\sim}{d} \tag{2.9}$$

A little manipulation of Eqs. (2.1), (2.3) and (1.4) shows that the stiffness of this element is given by

$$\underset{\sim}{K}_e = \int_{\Omega_e} \underset{\sim}{B}_b^T \, \underset{\sim}{D}_B \, \underset{\sim}{B}_b \, d\Omega + \underset{\sim}{P}_s^T \int_{\Omega_e} \underset{\sim}{B}_s^T \, \underset{\sim}{D}_s \, \underset{\sim}{B}_s \, d\Omega \, \underset{\sim}{P}_s \tag{2.10a}$$

where

$$\underset{\sim}{P}_s = \underset{\sim}{I} - \underset{\sim}{P}_b \tag{2.10b}$$

where $\underset{\sim}{I}$ is a unit matrix; Eqs. (1.1-3) and (2.4) give

$$\underset{\sim}{B}_b = \frac{1}{L} [-1, \quad +1, \quad 0, \quad 0] \tag{2.11a}$$

$$\underset{\sim}{B}_s = [\xi - 1, \quad -\xi, \quad -1/L, \quad 1/L] \tag{2.11b}$$

An interesting consequence of the fact that $\underset{\sim}{P}_s$ is a projection operator is that (see Stolarski and Belytschko (1985))

$$\underset{\sim}{P}_s \, \underset{\sim}{P}_s = \underset{\sim}{P}_s \tag{2.12}$$

so

$$\underset{\sim}{K}_e^s = \underset{\sim}{P}_s^T \int_{\Omega_e} \underset{\sim}{B}_s^T \underset{\sim}{D}_s \underset{\sim}{B}_s \, d\Omega \, \underset{\sim}{P}_s \tag{2.13a}$$

$$= \underset{\sim}{P}_s^T \int_{\Omega_e} \underset{\sim}{B}_{ss}^T \underset{\sim}{D}_s \underset{\sim}{B}_{ss} \, d\Omega \, \underset{\sim}{P}_s \tag{2.13b}$$

$$= \int_{\Omega_e} \underset{\sim}{B}_{ss}^T \underset{\sim}{D}_s \underset{\sim}{B}_{ss} \, d\Omega \tag{2.13c}$$

where

$$\underset{\sim}{B}_{ss} = \underset{\sim}{B}_s \underset{\sim}{P}_s = [-1/2, \quad -1/2, \quad -1/L, \quad +1/L] \tag{2.14}$$

The effect of the projection is thus to change the shear strain from a linear field such as given by the $\underset{\sim}{B}_s$-matrix of Eq. (2.11b) to the constant field given by (2.14).

Remark 2.1. It can be seen from (2.13c) and (2.14) that the stiffness matrix obtained by this procedure is identical to that obtained by reduced/selective integration by Hughes, et al. (1977).

Remark 2.2. Considerable leeway is available in the choice of the bending mode. We have chosen to ascribe all of the nodal rotations to the bending mode, but other choices are acceptable.

Remark 2.3. The linear displacement, linear rotation element is not subject to membrane locking, since $w^o_{,x}\, w_{,x}$ vanishes in (1.8) for that element.

The projection method for membrane locking is similar. In this case, the aim is to find the membrane strain ε^b so that in an inextensional mode of deformation, the membrane energy vanishes in Eq. (2.1). The projection for the linear-cubic beam element has been developed by Stolarski, et al. (1984a),

(1984b) and related to a mixed method by Belytschko, et al. (1985b). The displacement fields and initial deflection in this element are given by

$$u = u_1(1 - \xi) + u_2 \xi \tag{2.15a}$$

$$w = \phi_1 L (\xi^3 - 2\xi^2 + \xi) + \phi_2 L (\xi^3 - \xi^2) \tag{2.15b}$$

$$w^o = \phi_1^o \underbrace{L(\xi^3 - 2\xi^2 + \xi)}_{N_1} + \phi_2^o \underbrace{L(\xi^3 - \xi^2)}_{N_2} \tag{2.15c}$$

Note again that we have used a corotational coordinate system so that the x axis always connects node 1 to node 2.

The stiffness matrix for this element is obtained by using (1.1-2) in conjunction with (2.1) which yields

$$\underset{\sim}{K}_e = \int_{\Omega_e} \underset{\sim}{B}_b^T \underset{\sim}{D}_B \underset{\sim}{B}_b \, d\Omega + \underset{\sim}{P}_m^T \int \underset{\sim}{B}_m \underset{\sim}{D}_M \underset{\sim}{B}_m \, d\Omega \, \underset{\sim}{P}_m \tag{2.16}$$

where

$$\underset{\sim}{B}_b = [0, -N_{1,xx}, -N_{2,xx}] \tag{2.17a}$$

$$\underset{\sim}{B}_m = [\frac{1}{L}, w^o(x)N_{1,x}, w^o(x)N_{2,x}] \tag{2.17b}$$

$$\underset{\sim}{d}^T = [u_2 - u_1, \phi_1, \phi_2] \tag{2.17c}$$

If $\underset{\sim}{P}_m = \underset{\sim}{I}$, or in other words, if no projection is used, then this element will lock. The cause of locking can be understood by simply considering $\underset{\sim}{B}_m$; if the

moment on an element is constant, then $\phi_1 = -\phi_2$, so if $w_o(x) \neq 0$, then the constant term 1/L cannot negate the terms $w^o(x)N_{i,x}$, hence parasitic membrane strains will arise. If $w^o(x) = 0$, the beam is straight and no coupling exists between flexural and membrane effects. This coupling is an important attribute of curved elements.

The projection operator which eliminates locking is developed in Stolarski, et al. (1984) to be

$$\underset{\sim}{P}_m = \begin{bmatrix} 1 & \frac{L}{30}(-4\phi_1^o + \phi_2^o) & \frac{L}{30}(\phi_1^o - 4\phi_2^o) \\ 0 & 0 & 0 \\ 0 & 0 & 0 \end{bmatrix} \qquad (2.18)$$

This projection is obtained by noting that the change in the chord length $u_{21}^b \equiv u_2^b - u_1^b$ in a pure bending mode is given by

$$u_{21}^b = \int_0^L - w^o\, w_{,xx}\, dx = \frac{L}{30}(-4\phi_1^o + \phi_2^o)\phi_1 + \frac{L}{30}(\phi_1^o - 4\phi_2^o)\phi_2 \qquad (2.19)$$

As can be seen from Fig. 3, this change in chord length is required to maintain an inextensible midline during bending of a curved element; if an element is straight, no change in chord length occurs during bending.

An analogous approach has also been used to formulate a triangular shell element in Stolarski, et al. (1984) which is here called DKT-CST*. In its development, it is convenient to use only deformational degrees of freedom. Following Argyris (1965), the membrane state of strain is expressed in terms of the elongations of the 3 sides n_I and the bending state represented by deformation rotations γ_{II}, so that the deformational d.o.f. are

$$\underset{\sim}{n}^T = [n_1, n_2, n_3] \tag{2.20a}$$

$$\underset{\sim}{\phi} = [\phi_{x1}, \phi_{y1}, \phi_{x2}, \phi_{y2}, \phi_{x3}, \phi_{y3}] \tag{2.20b}$$

The strain energy of the element is then given by

$$U = \frac{1}{2} \underset{\sim}{\phi}^T \underset{\sim}{K}_b \underset{\sim}{\phi} + \frac{1}{2} (\underset{\sim}{n} - \underset{\sim}{n}_b)^T \underset{\sim}{K}_m (\underset{\sim}{n} - \underset{\sim}{n}_b) \tag{2.21}$$

where $\underset{\sim}{K}_b$ and $\underset{\sim}{K}_m$ are the bending and membrane stiffnesses, respectively. On the element labeled DKT-CST*, in Section 6, the discrete Kirchhoff triangle (DKT) element of Batoz (1982) is used for the bending stiffness and the constant strain element is used for membrane stiffness. Note that in the absence of $\underset{\sim}{n}_b$ in (2.21), the bending and membrane behavior of the element are totally uncoupled.

The bending elongation along each side is now given by the same equations as for the beam, (2.19), but written in the form

$$n_{Ib} = \frac{L_I}{30} (-4\phi^o_{1I} + \phi^o_{2I})\phi_{1I} + \frac{L_I}{30} (\phi^o_{1I} - 4\phi^o_{2I})\phi_{2I} \tag{2.22}$$

where ϕ_{1I} and ϕ_{2I} are the rotations relative to side I of the element and ϕ^o_{1I}, ϕ^o_{2I} are the initial slopes of the shell surface relative to the chord of the element. From the relations (2.22) at the three sides, the projection operator $\underset{\sim}{P}_m$ is obtained.

Details of the element are given in Stolarski, et al. (1984). One important aspect of the formulation which was inadvertently omitted from that paper is that ϕ^o_{iI} and ϕ_{iI} in (2.22) must be defined so that the bending

elongations of the common edge of two contiguous elements are identical. Otherwise, the projections for elements which are not coplanar will be different, and as a consequence, parasitic membrane energy will appear in a state of pure bending. This is accomplished by defining ϕ_{iI} as the rotation in the plane defined by side I and the normal to the shell at node i.

It can be seen from (2.22) that the bending part of the elongation couples the membrane response with the rotations, and hence, as in the beam, adds membrane/flexural coupling to the element.

3. RELATION BETWEEN MIXED AND MODE-DECOMPOSITION PROJECTION METHODS

In this Section a simple form of the element stiffness matrix for mixed methods will be developed and then compared to the explicit projection method to illustrate their similar structure. The Hu-Washizu variational principle will be used to develop the mixed method. This principle can be written for a single element in the form

$$\int_{\Omega} [\delta\varepsilon_{ij} (D_{ijk\ell}\, \varepsilon_{k\ell} - \sigma_{ij}) - \delta\sigma_{ij}(\varepsilon_{ij} - u_{(i,j)}) + \delta u_{(i,j)}\, \sigma_{ij}]d\Omega = \sum_{I=1}^{n_N} \delta u_{iI}\, f_{iI} \tag{3.1}$$

Standard indicial notation has been used, with repeated lower case subscripts summed over their range; commas denote partial derivatives. Upper case subscripts pertain to degrees of freedom of the n_N nodes. The nomenclature in this section is as follows:

ε_{ij} ,	$\underset{\sim}{\varepsilon}$	=	strain; matrix form $\underset{\sim}{\varepsilon}$ is considered a column matrix such as $\underset{\sim}{\varepsilon}^T = (\varepsilon_x, \varepsilon_y, 2\varepsilon_{xy})$
σ_{ij} ,	$\underset{\sim}{\sigma}$	=	stress matrix
u_i ,	$\underset{\sim}{u}$	=	displacement field
$\underset{\sim}{d}_I$,	$\underset{\sim}{d}$	=	nodal displacements
$u_{(i,j)}$,	$\nabla^s \underset{\sim}{u}$	=	symmetric part of the gradient of the displacement field
$D_{ijk\ell}$,	$\underset{\sim}{D}$	=	stress-strain matrix

In the above, both the subscripted tensor forms and the matrix forms commonly used in finite element implementation are listed. Through the use of the

latter form, the relation of the projection method and Hu-Washizu can be clarified more easily. The displacement field in this principle must be C^0, while the strain and stress fields may be C^{-1}.

The three independent fields are approximated by interpolation functions as follows

$$u_i = \sum_{I=1}^{n_D} N_{iI}\, d_I \qquad \text{or} \qquad \underset{\sim}{u} = \underset{\sim}{N}\, \underset{\sim}{d} \tag{3.2a}$$

$$\varepsilon_{ij} = \sum_{I=1}^{n_E} E_{ijI}\, e_I \qquad \text{or} \qquad \underset{\sim}{\varepsilon} = \underset{\sim}{E}\, \underset{\sim}{e} \tag{3.2b}$$

$$\sigma_{ij} = \sum_{I=1}^{n_E} S_{ijI}\, s_I \qquad \text{or} \qquad \underset{\sim}{\sigma} = \underset{\sim}{S}\, \underset{\sim}{s} \tag{3.2c}$$

where n_D are the number of displacement d.o.f. and n_E are the number of strain (or stress) interpolants. An important part of this presentation is the use of mnemonic terms for the strain and stress interpolants and coefficients so that they are easily recognized later. We also define the standard $\underset{\sim}{B}$-matrix through

$$u_{(i,j)} = \sum_{I=1}^{n_D} B_{ijI}\, d_I \qquad \text{or} \qquad \nabla^S \underset{\sim}{u} = \underset{\sim}{B}\, \underset{\sim}{d} \tag{3.2d}$$

Substituting the above into Eq. (3.1), and using the arbitrariness of the appropriate variations yields:

strain-displacement equations

$$\sum_{J=1}^{n_E} \bar{E}_{IJ}\, e_J = \sum_{J=1}^{n_D} \bar{B}_{IJ}\, d_J \qquad \text{or} \qquad \underset{\sim}{\bar{E}}\, \underset{\sim}{e} = \underset{\sim}{\bar{B}}\, \underset{\sim}{d} \tag{3.3}$$

stress-strain equations

$$\sum_{J=1}^{n_E} \bar{D}_{IJ}\, e_J = \sum_{J=1}^{n_E} \bar{E}^T_{IJ}\, s_J \qquad \text{or} \qquad \underset{\sim}{\bar{D}}\, \underset{\sim}{e} = \underset{\sim}{\bar{E}}^T\, \underset{\sim}{s} \tag{3.4}$$

equilibrium

$$f_I = \sum_{J=1}^{n_E} \bar{B}^T_{IJ}\, s_J \qquad \text{or} \qquad \underset{\sim}{f} = \underset{\sim}{\bar{B}}^T\, \underset{\sim}{s} \tag{3.5}$$

where

$$\bar{E}_{IJ} = \int_\Omega S_{ijI}\, E_{ijJ}\, d\Omega \tag{3.6a}$$

$$\bar{B}_{IJ} = \int_\Omega S_{ijI}\, B_{ijJ}\, d\Omega \tag{3.6b}$$

$$\bar{D}_{IJ} = \int_\Omega E_{ijI}\, D_{ijk\ell}\, E_{k\ell J}\, d\Omega \tag{3.6c}$$

At this point it is convenient to note that

$$\underset{\sim}{E} = [\underset{\sim}{E}_1, \underset{\sim}{E}_2, \ldots \underset{\sim}{E}_{nE}] \tag{3.7a}$$

$$\underset{\sim}{S} = [\underset{\sim}{S}_1, \underset{\sim}{S}_2, \ldots S_{nE}] \tag{3.7b}$$

In terms of this notation, (3.6) can be rewritten as

$$\bar{E}_{IJ} = \int_{\Omega} \underset{\sim}{S}_I^T \underset{\sim}{E}_J \, d\Omega \tag{3.8a}$$

$$\bar{B}_{IJ} = \int_{\Omega} \underset{\sim}{S}_I^T \underset{\sim}{B}_J \, d\Omega \tag{3.8b}$$

$$\bar{D}_{IJ} = \int_{\Omega} \underset{\sim}{E}_I^T \underset{\sim}{D} \underset{\sim}{E}_J \, d\Omega \tag{3.8c}$$

From this notation it becomes clear that the essential ingredients of the mixed method, such as the $\bar{B}$-matrix, are simply the projections of these matrices onto the corresponding stress and strain interpolants. The $\underset{\sim}{B}$-matrix, for example, is projected onto the stress interpolants in this mixed method.

A more revealing form of the mixed method can be obtained by orthogonalizing the strain and stress interpolants so that

$$\bar{E}_{IJ} = \int_{\Omega} S_{ijI} \, E_{ijI} \, d\Omega = I_{IJ} \qquad \text{or} \qquad \underset{\sim}{\bar{E}} = \underset{\sim}{\bar{I}} \tag{3.9}$$

where $\underset{\sim}{I}$ is the unit matrix. This can always be achieved by a Gram-Schmidt procedure if the stress and strain interpolants span the same space and are linearly independent; it is also convenient if each strain (or stress) parameter e_I (or s_I) pertains only to a single strain ε_{ij} (or stress σ_{ij}). Using (3.9), Eqs. (3.3 - 5) can be written

$$\underset{\sim}{e} = \underset{\sim}{\bar{B}} \, \underset{\sim}{d} \tag{3.10a}$$

$$\underset{\sim}{s} = \underset{\sim}{\bar{D}} \, \underset{\sim}{e} \tag{3.10b}$$

$$\underset{\sim}{f} = \overline{\underset{\sim}{B}}^T \underset{\sim}{s} \tag{3.10c}$$

which can easily be recognized as the strain - displacement, constitutive and nodal-force stress (equilibrium) relations in projected form.

The element stiffness matrix is now obtained by combining (3.4-6), which is most easily done with the matrix form, and gives

$$\underset{\sim}{f} = \overline{\underset{\sim}{B}}^T (\overline{\underset{\sim}{E}}^T)^{-1} \overline{\underset{\sim}{D}} (\overline{\underset{\sim}{E}}^{-1}) \overline{\underset{\sim}{B}} \underset{\sim}{d} \tag{3.11}$$

Using the orthogonality (3.9), (3.11) can then be written as

$$\underset{\sim}{K}_e = \overline{\underset{\sim}{B}}^T \overline{\underset{\sim}{D}} \overline{\underset{\sim}{B}} \tag{3.12}$$

For purposes of comparison of the mixed method with the mode decomposition projection method developed in Section 2, it is also worthwhile to write (3.12) using the definition of $\overline{D}_{IJ}$, (3.8c), which gives

$$\underset{\sim}{K}_e = \overline{\underset{\sim}{B}}^T \int_\Omega \underset{\sim}{E}^T \underset{\sim}{D} \underset{\sim}{E} \, d\Omega \, \overline{\underset{\sim}{B}} \tag{3.13}$$

Table 1 compares the above form with the mode decomposition projection method. It can be seen that the two methods are identical in structure, with the matrix $\underset{\sim}{P}$ playing the role of the projection of $\underset{\sim}{B}$ onto the stress interpolant $\underset{\sim}{S}$, hence the name stress-projection.

In many elements, the same interpolation functions are used for the stresses and strains. To establish the equivalence of the two methods, the strain interpolants should be orthogonalized, and the matrix $\underset{\sim}{P}$ plays the role of the projection of the $\underset{\sim}{B}$ matrix onto the strain interpolant $\underset{\sim}{E}$.

Although the conditions for equivalence between mode decomposition projection methods and mixed methods appears straightforward, establishing the exact equivalence is not possible in some elements. Stolarski and Belytschko (1985a) have shown an equivalence between mode decomposition projection methods and mixed methods for a large variety of beam elements, but in that paper it was shown that no mixed element is equivalent to the triangular plate element developed in Belytschko, et al. (1984c).

Remark. The equivalence of the two methods does not depend on the orthogonality of the strain and stress interpolants; it only serves to clarify the relationship. The stiffness matrix in fact is not changed by orthogonalization of the interpolants.

Table 1

Comparison of Mode Decomposition Projection and Mixed Methods

Mixed Method	Mode Decomposition Projection Method
(Orthogonal Interpolants)	
Strains	
See Eqs. (3.2b), (3.10a)	
$\underset{\sim}{\varepsilon} = \underset{\sim}{E}\,\underset{\sim}{e} = \underset{\sim}{E}\,\overline{\underset{\sim}{B}}\,\underset{\sim}{d}$	$\underset{\sim}{\varepsilon} = \underset{\sim}{B}_s\,\underset{\sim}{P}_s\,\underset{\sim}{d}$
Stiffness Matrix	
See Eq. (3.13)	See Eq. (2.10a) (only shear stiffness)
$\underset{\sim}{K}_e = \overline{\underset{\sim}{B}}^T \int \underset{\sim}{E}^T \underset{\sim}{D}\,\underset{\sim}{E}\,d\Omega\,\overline{\underset{\sim}{B}}$	$\underset{\sim}{K}_e = \underset{\sim}{P}_s^T \int \underset{\sim}{B}_s^T \underset{\sim}{D}_s\,\underset{\sim}{B}_s\,d\Omega\,\underset{\sim}{P}_s$

Note interchangeability when $\overline{\underset{\sim}{B}} = \underset{\sim}{P}_s$, $\underset{\sim}{E} = \underset{\sim}{B}_s$.

4. NINE-NODE LAGRANGE SHELL ELEMENT

The 9-node shell element to be discussed here has been extensively studied by Parish (1979) and by Hughes and Liu (1981). It is a Mindlin type, degenerated shell element which uses quadratic Lagrange interpolants. The 2x2 quadrature version of the 9-node element possesses the unique and beneficial property that in constant moment states, the transverse shear and membrane stresses (that is, the parasitic stresses), vanish at the quadrature points. Thus 2x2 quadrature provides a stress projection which should avoid locking.

This property can be verified by performing the numerical experiments illustrated in Fig. 4. As indicated in the figure, both flat elements and elements with a single curvature were considered. In the numerical experiment, moments were applied as shown and the transverse shear energy and membrane energy was monitored. In all cases which were tried, the transverse shear and membrane energies were less than 0.01% of the total strain energy.

The same behavior was observed when the quadrature points were shifted from $\eta = \xi = \pm 3^{-1/2}$ (the Gauss points) to $\eta = \xi = \pm 1/2$. However, the accuracy of the element then deteriorates even though the membrane energy locking does not occur; for an illustration of this see Table 2, which gives results for the arch problem described in Fig. 1b. These runs were made with a beam element because the shell develops a spurious mode for the $\pm 1/2$ quadrature scheme.

This feature of the 9-node element with 2x2 quadrature makes it a very desirable element for the analysis of shells. Its highly convergent behavior will be illustrated in Section 6. However, the element suffers from one important drawback: its rank is not sufficient to preclude spurious singular modes, so for some boundary conditions the total stiffness matrix is singular.

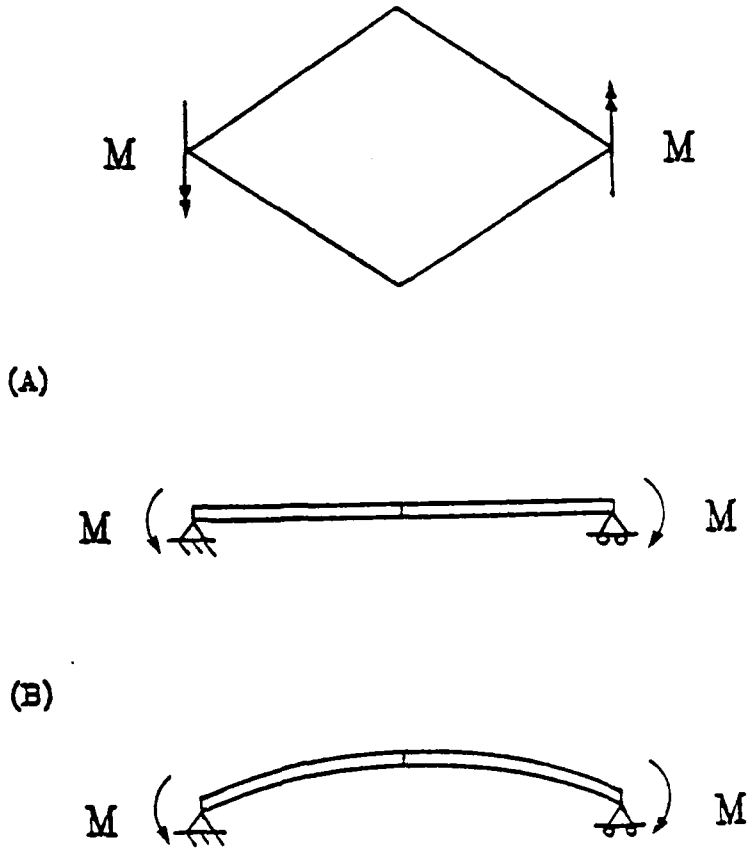

Figure 4. Bending test for an element.

Table 2

Effect of Quadrature Point Location on Accuracy for the Arch Problem

Number of Elements	w^{FEM}/w^{exact}	U_m/U	U_s/U
Gauss quadrature $\xi = \pm 3^{-1/2}$			
10	0.9861	0.0013	0.0031
20	0.9984	0.0013	0.0031
40	1.0009	0.0013	0.0031
Midpoint quadrature $\xi = \pm 1/2$			
10	1.0928	0.0016	0.8033
20	1.0257	0.0120	0.0041
40	1.0077	0.4199	0.0031

U_m = membrane energy, U_s = shear energy, U = total energy

w = deflection under load

The control of these spurious modes has been developed for the 9-node plate element in Belytschko, et al. (1984), and the stabilization procedure for the shell element has been reported without analysis in Belytschko, et al. (1985). In Appendix A a description of the element as used here and a detailed development of the stabilization operator is given.

Reduced integration of the stiffness may also be viewed as a projection method. This, of course, is suggested by the equivalence principle of Malkus and Hughes (1978) which establishes the equivalence of reduced integration displacement and reduced integration mixed methods; the relationship between the latter and projection methods has already been discussed herein. Reduced integration represents an <u>implicit</u> projection, in that the projection operator is never explicitly invoked. An exact mixed formulation for the 9-node (2x2) element is developed in Appendix B. In that development, by using Dirac functions for the stresses, the reduced quadrature displacement formulation can be shown to be equivalent to an <u>exactly</u> integrated mixed element.

5. AN OBSTACLE COURSE FOR SHELL ELEMENTS

A major shortcoming which has impaired the development of shell elements is that in the reports on many elements, they are not tested against a set of problems which challenge even a fraction of the capabilities required in a high-performance element. A good shell element must have the ability to handle inextensional bending modes of deformation, rigid body motion without straining, and complex membrane states of stress. Inadequacies in this spectrum of attributes are a severe handicap.

A useful obstacle course for an element must also be reasonably short; it is useless to include problems which only disqualify elements which are already disqualified by other problems.

In this effort, we have assembled the three test problems shown in Fig. 5. All of these problems have been seperately used by others in the literature as noted in Table 3. We have found that together they are an extremely discriminating set of problems.

Some remarks on this selection:

1. The Scordelis-Lo problem is extremely useful for determining the ability of an element to accurately solve complex states of membrane strain. A substantial part of the strain energy is membrane strain energy, so the representation of inextensional modes is not crucial in this problem. Even elements with severe membrane locking will converge at a moderate rate in this test, whereas inadequacie· in membrane stress accuracy will severely inhibit convergence.
2. The pinched cylinder with a diaphragm is one of the most severe tests for both inextensional bending modes and complex membrane states. We have not

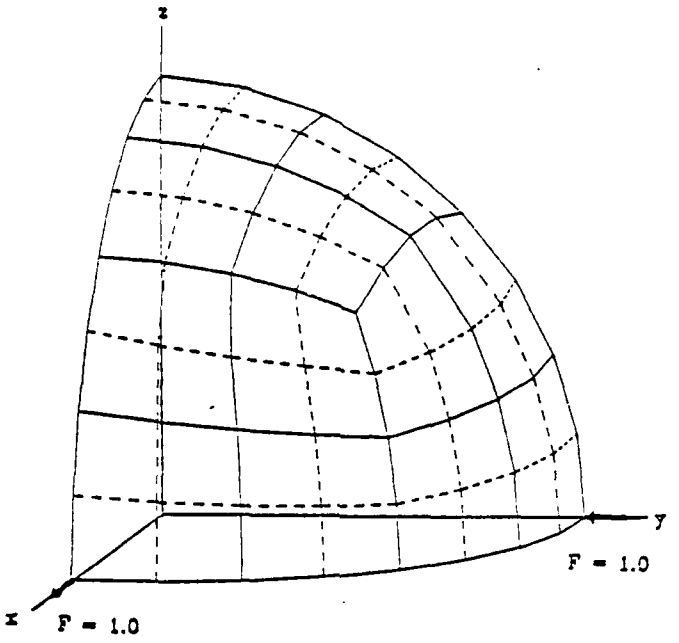

Hemispherical Shell

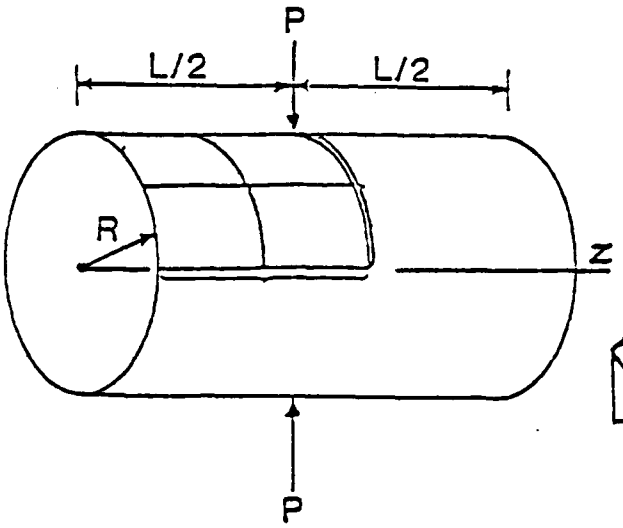

Pinched Cylinder with Diaphragm

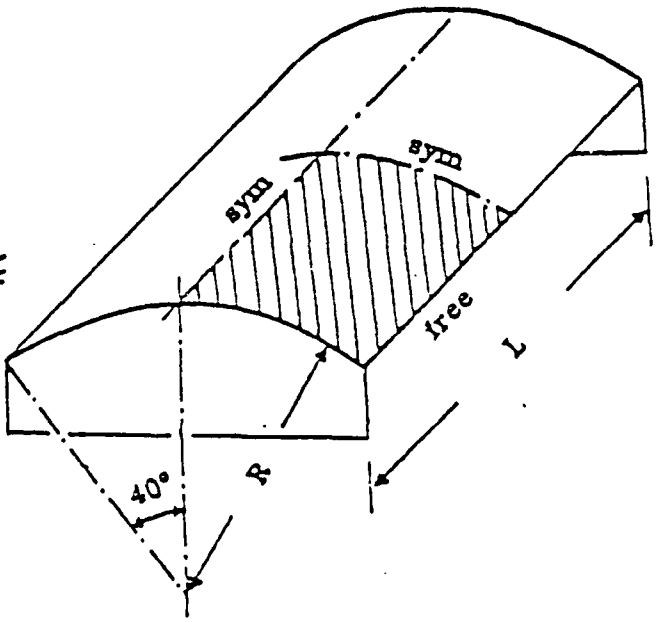

Scordelis–Lo Roof

Figure 5. Obstacle course for shell element.

included the pinched cylinder with free ends because any element that passes the diaphragm support test will perform well when the boundary condition is simplified to a free boundary.

3. The hemispherical shell problem is again a challenging test of an element's ability to represent inextensional modes; it exhibits almost no membrane strains. The role of this test problem is less critical with regard to inextensional bending than the pinched cylinder problem. However, it is a very useful problem for checking the ability of the element to handle rigid body rotations about normals to the shells surface. Large sections of this shell rotate almost as rigid bodies in response to this load, so that the ability to accurately model rigid body motion is essential for good performance in this problem. Some 5 d.o.f. per node formulations of triangular elements fail this test because they result in spurious straining when rotated about the normal to the shell surface. This problem is much more challenging than the point-loaded spherical problem which is often used.

Table 3

Problem Parameters for Obstacle Course

Problem 1. Scordelis - Lo Roof
length: $L = 50.0$
radius: $R = 25.0$
thickness: $t = 0.25$
Young's modulus: $E = 4.32 * 10^8$
Poisson's ratio: $\nu = 0.0$
boundary conditions: supported at each end by rigid diaphragms
loading: uniform vertical gravity load of 90.0 per unit area
converged numerical solution: vertical displacement at midside of free edge = 0.3024
reference: Scordelis and Lo (1969), Ashwell (1976)

Problem 2. Pinched Cylinder with Diaphragms
length: $L = 600.0$
radius: $R = 300.0$
thickness: $t = 3.0$
Young's modulus: $E = 3.0 * 10^6$
Poisson's ratio: $\nu = 0.3$
boundary conditions: constrained at each end by a rigid diaphragm, $u_x = u_y = \phi_z = 0$ in Fig. 5
loading: opposing radial loads as shown in Fig. 5, $F = 1.0$
radial displacement at point load: $0.18248 * 10^{-4}$
references: Lindberg, et al. (1969), Dvorkin and Bathe (1984), Flugge (1973)

Problem 3. Hemispherical Shell
radius: $R = 10.0$
thickness: $t = 0.04$
Young's modulus: $E = 6.825 * 10^7$
Poisson's ratio: $\nu = 0.3$
boundary condition: bottom circumferential edge of hemisphere is free
loading: opposing radial point loads alternating at 90° as shown in Fig. 5, $F = \pm 2.0$
solution: radial displacement at loaded points: 0.0924
references: Morley and Morris (1978), MacNeal and Harder (1984)

Table 4

Comparison of Results for Hemispherical Shell (See Fig. 2)

with Consistent and Inconsistent Spurious Mode Control

(results given are ratio of computed to analytic displacement under load)

Mesh for Quarter of Shell (number of nodes/edge)	Consistent Control γ given by Eq.(A.32)	Inconsistent Control $\gamma = \underline{h}$	2x2 Quadrature $\gamma = \underline{Q}$
3	1.319	1.2672	-
5	1.0794	1.0792	1.0954
9	1.0056	1.0063	1.0138
13	0.9963	0.9970	1.0037
17	0.9925	0.9958	0.9987

Remark 5.1. This selection of shell problems was inspired by the work of MacNeal and Harder (1984), who devised a set of standard finite element problems which included hemispherical shell and the Scordelis Lo roof, but not the pinched cylinder. They also included various plane patch tests and plane, two dimensional problems.

6. RESULTS

Results have been obtained with two classes of elements: 3-node triangular elements with 5 or 6 d.o.f. per node and C^0 Mindlin type shell elements based on a degenerate shell theory of Hughes and Liu (1981). All of the triangular elements utilize the discrete Kirchhoff triangle (DKT) formulation of Batoz et al. (1982) with different membrane strain fields. They are as follows:

1. DKT - CST: a standard flat triangle with constant membrane strains and no membrane/bending coupling.
2. DKT - CST*: a constant strain triangle is used for the membrane strain as above but the membrane projection described in Section 2 and originally reported by Stolarski et al. (1984), which couples membrane and bending, is added.
3. DKT - LST: a 6 d. o. f. per node element in which a linear membrane field with reduced integration as given by Carpenter et al. (1985) is employed for the membrane effects. This element is flat and has no membrane-flexural coupling.
4. DKT - Olson-Bearden: a linear field given by Olson and Bearden (1979) is used for the membrane strains in combination with a DKT element. This element has 6 d.o.f per node and no membrane flexural coupling.

Among the Mindlin C^0 elements, the following were used:

1. 4-node SRI: this is a standard 4-node Mindlin element described by Hughes and Liu (1981) with selective reduced integration, consisting of reduced integration on shear (1 point) and 2x2 quadrature on the bending and membrane terms.

2. 9-node SRI: the 9-node Lagrange element with 3x3 quadrature on all bending and membrane terms and 2x2 quadrature on the shear terms.
3. 9-node 3x3: full quadrature (3x3) on all stiffness terms of the 9-node element.
4. 9-node γ-method: 2x2 quadrature on all terms of the element stiffness with γ-stabilization, as described in Appendix A.

Scordelis-Lo roof. Results for this problem shown in Fig. 6. These are observations of element performance for this problem:

1. The DKT-CST and DKT-CST* are both very poor for this problem, whereas for the other problems in this obstacle course they perform very well.
2. Among the triangles, only the Olson-Bearden and DKT-LST elements perform reasonably.
3. The 9-node γ-element and the 4-node SRI elements perform extremely well on this problem. However, when a selective reduced integration is used in this element, the results hardly differ from full integration. This is very puzzling, since the problem is dominated by membrane response rather than bending, so the severe locking of 9-node SRI element is quite unexpected. In fact, there seems to be considerable membrane locking in the coarse meshes, but it is quickly eliminated with mesh refinement.

Pinched cylinder with diaphragm. Results for this problem are given in Fig. 7. In this problem, all of the triangular elements work reasonably well, with only the DKT-CST being marginal. On the other hand, the performance of all of the Mindlin elements, except the 9-node γ-element, are quite poor. Particularly noteworthy is the fact that even with 17 nodes along each edge, the 4-node SRI element is still 5% in error and converging very slowly. This is the only problem in this set in which the 4-node element performs below

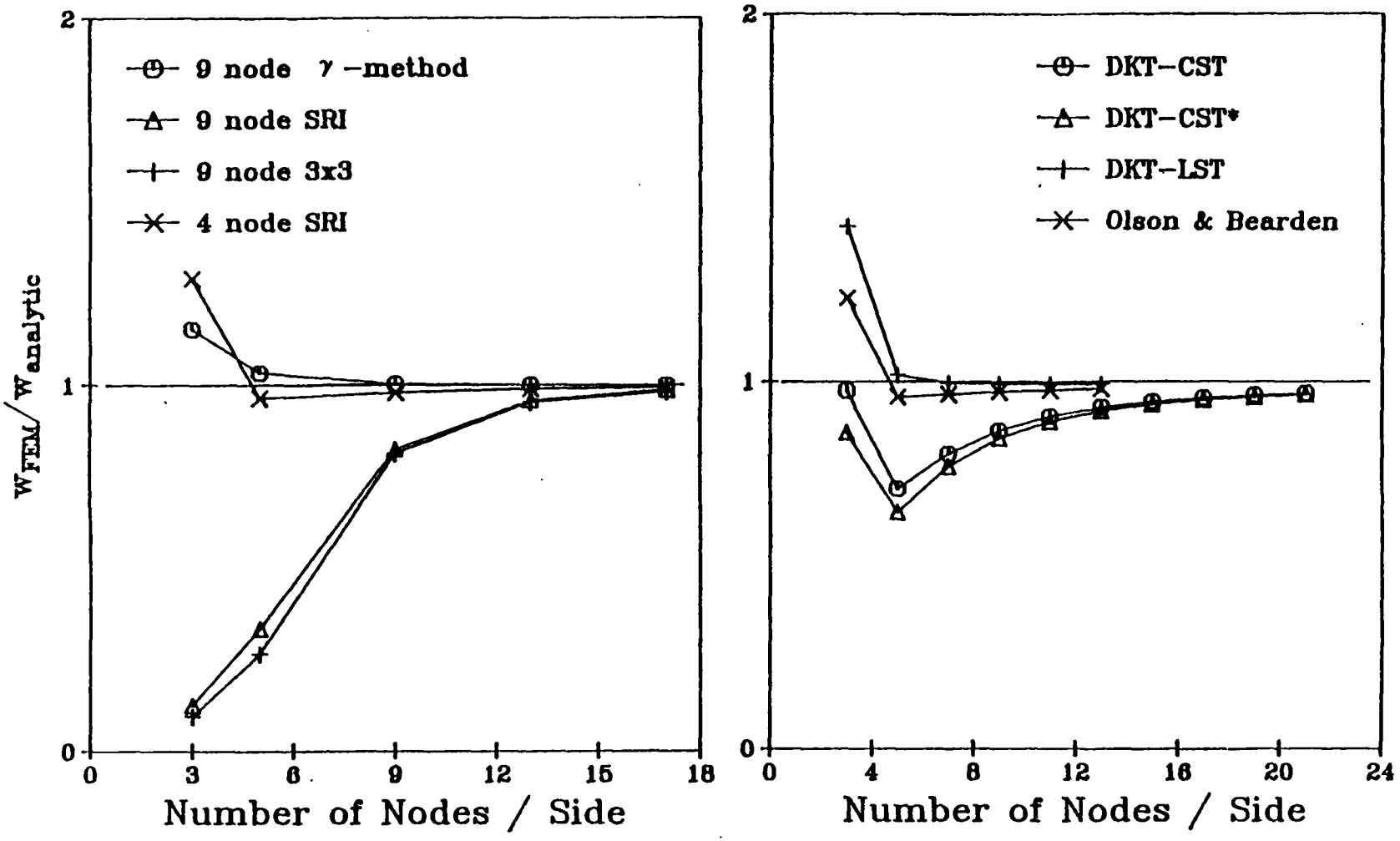

Figure 6. Scordelis Lo roof; vertical deflection at midpoint of free edge is compared with converged solution.

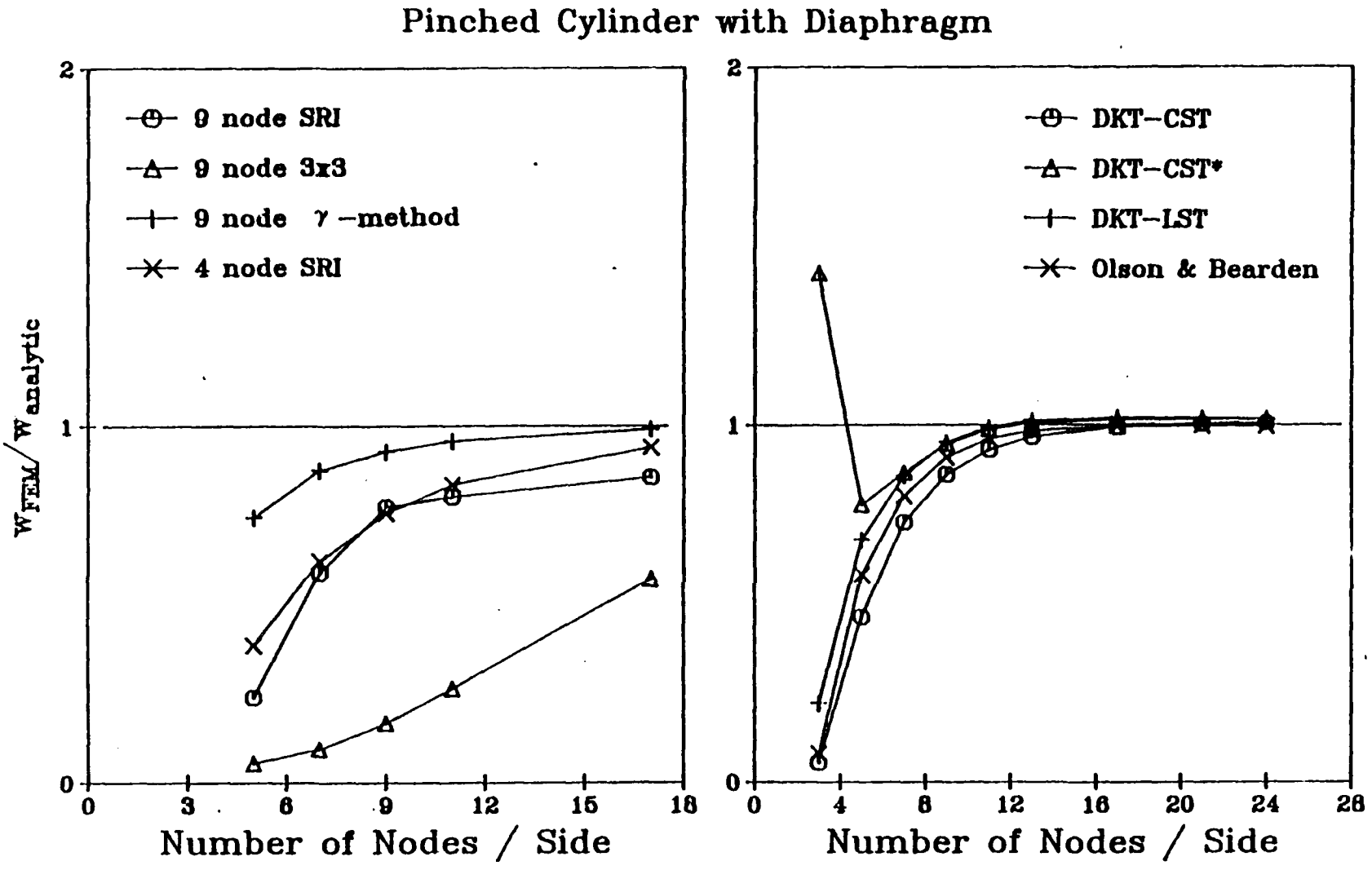

Figure 7. Pinched cylinder with diaphragm; deflection under load compared with analytic solution.

par. No improvement is achieved in the 4-node element by using 1-point quadrature on all terms, see Liu et al. (1985).

In order to illustrate the relative magnitudes of shear and membrane locking, Fig. 8 shows the results obtained for the 9-node element for SRI, 2x2, and 3x3 quadrature. It can be seen that for coarse meshes, membrane locking is dominant whereas for the finest meshes, shear locking becomes more important.

Figure 9 clarifies the role of membrane and shear locking by showing the fractions of the total energy which are shear and membrane energies for various meshes of 9 and 4-node elements. As can be seen, for all of the elements, the shear energy tends to almost zero as the meshes are refined, but the rate of convergence of the shear energy for the 9-node 3x3 element is quite slow. The membrane energy fraction of the γ-element tends to approximately 0.373. For the 4-node SRI element the membrane energy is somewhat larger for all of the meshes considered.

For the 9-node 3x3 element, the membrane energy is overpredicted even for the most refined mesh, which is indicative of membrane locking. The initial increase of the membrane-energy fraction, which is apparent in Fig. 9, is somewhat puzzling. Evidently for the coarse meshes, the total internal energy is very small because of severe locking; the initial refinement of the mesh in this element serves primarily to reduce shear locking, so that parasitic membrane energy actually increases at first.

Spherical shell problem. The results for the spherical shell are shown in Fig. 10. The following points are noteworthy:

1. This is the only problem in which the Olson-Bearden element performs poorly.

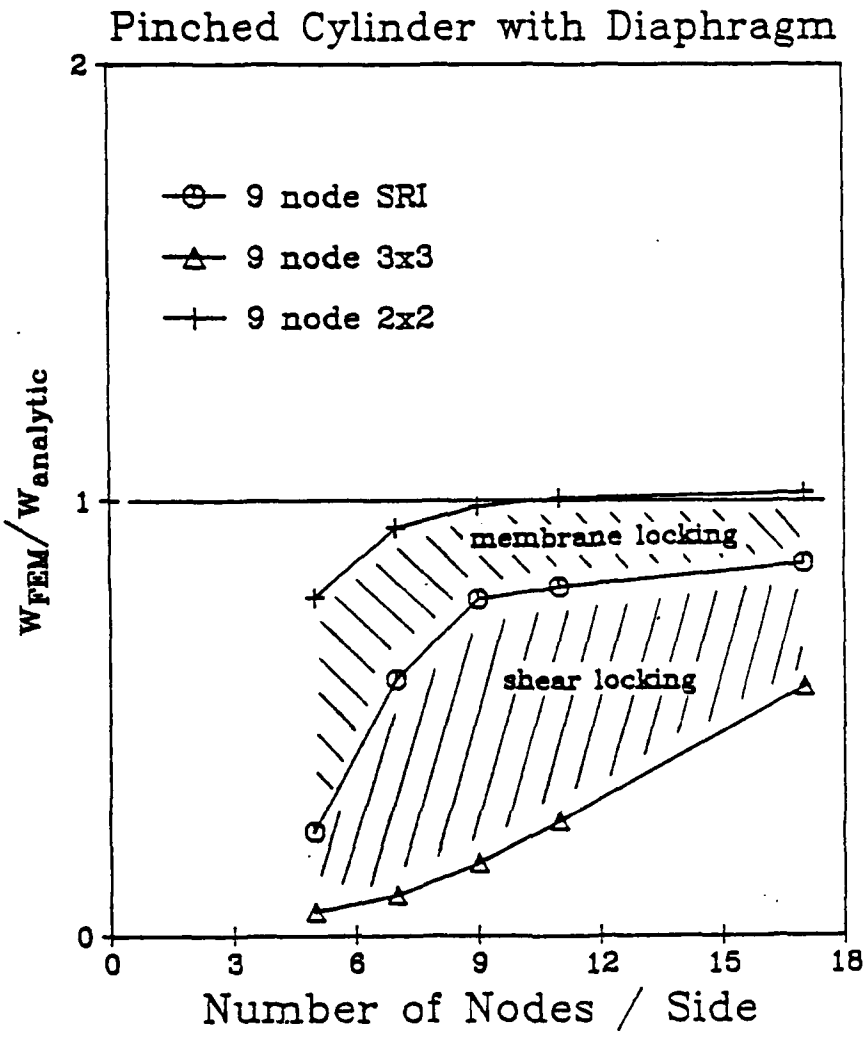

Figure 8. Relative effects of shear and membrane locking in pinched cylinder with diaphragm.

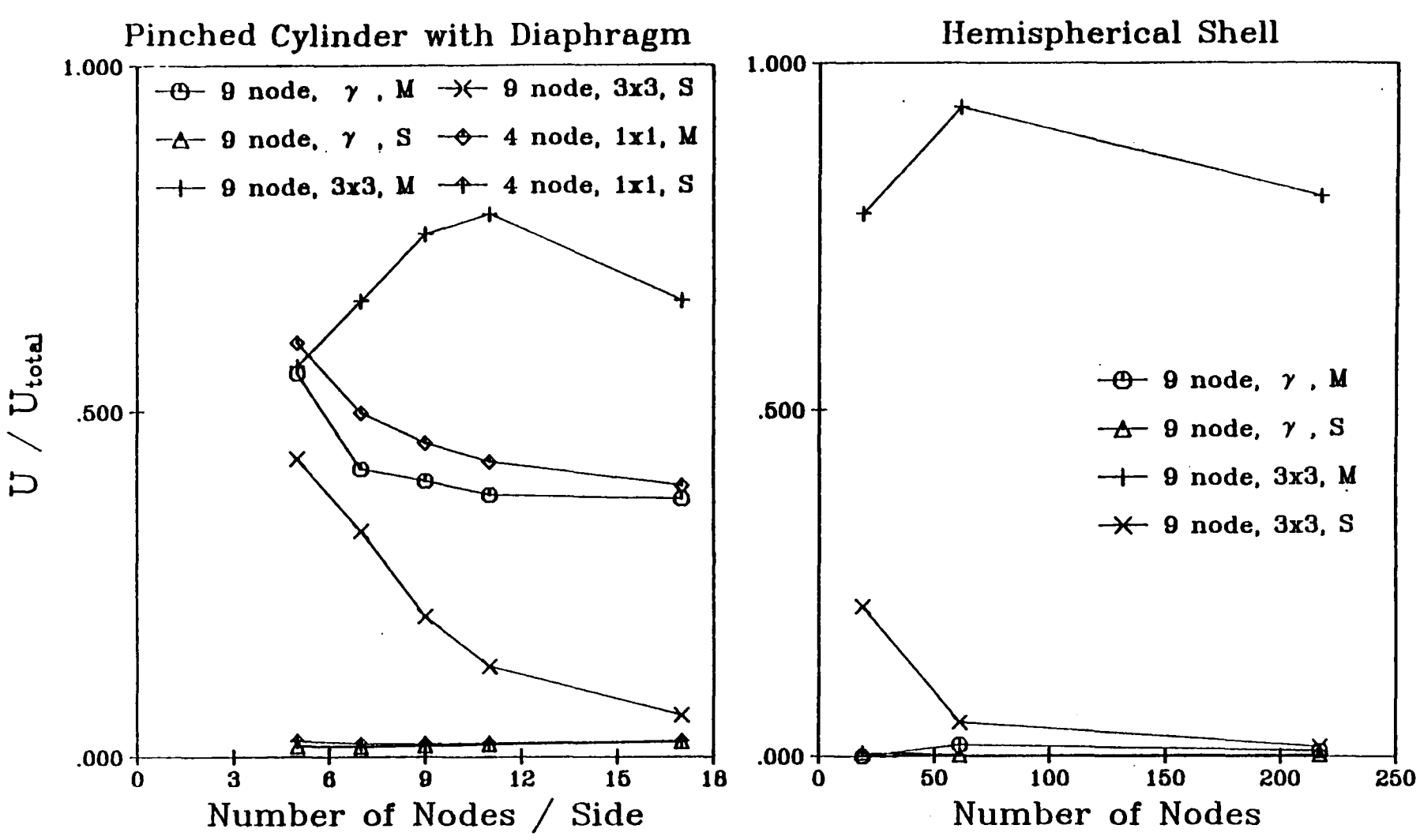

Figure 9. Partition of strain energy into membrane (M) and shear energy (S) for the 9-node element in the pinched cylinder/diaphragm and hemispherical shell problems.

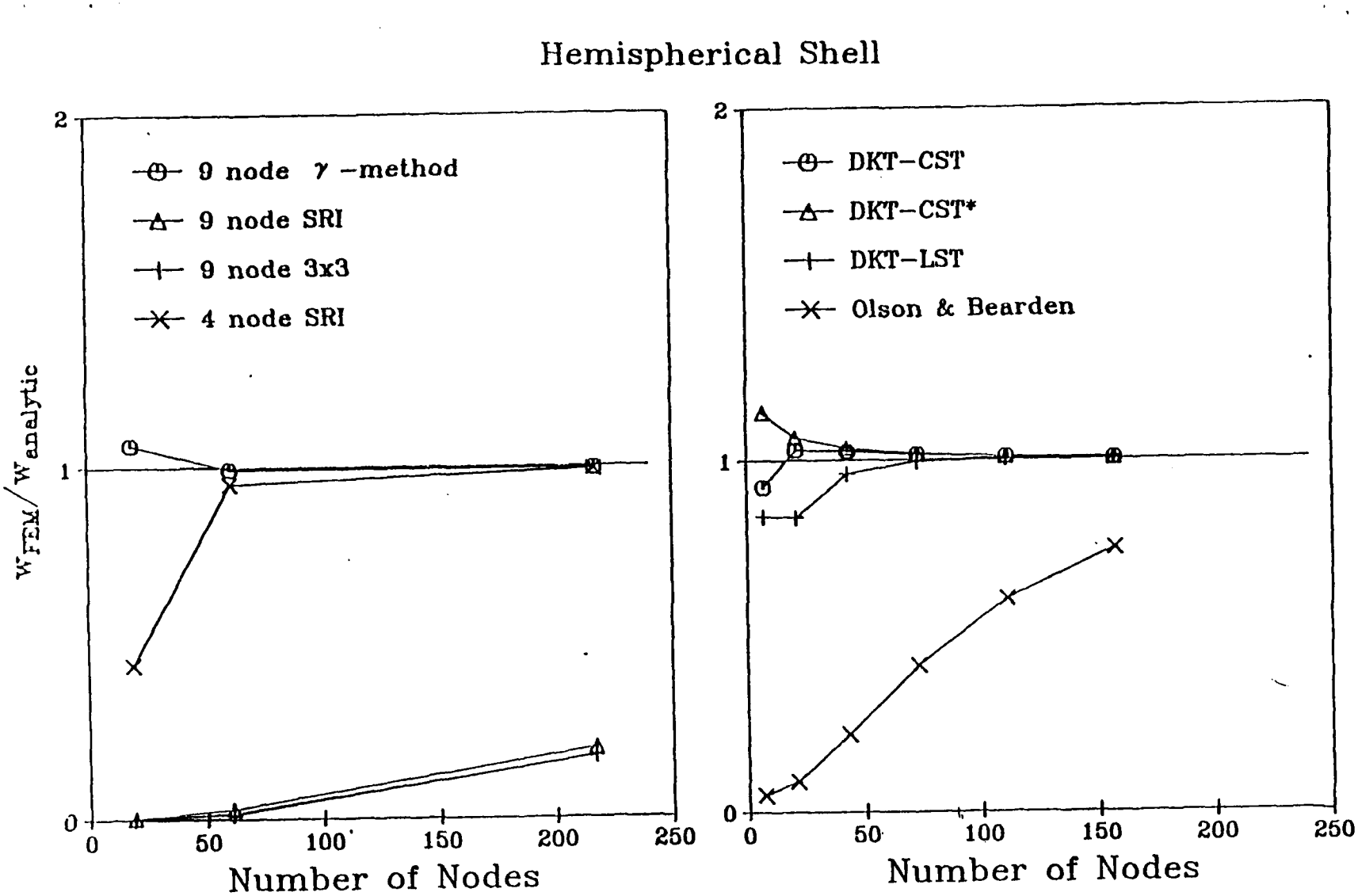

Figure 10. Hemispherical shell problem; deflection under load compared with analytic Solution.

2. The other triangular elements perform extremely well in this problem, whereas the fully integrated C^0 elements (4-node and 9-node) all exhibit severe membrane locking. Shear locking is almost totally absent.

Remark 6.1: Noor and Peters (1981) have shown similarly stiff behavior of displacement elements for curved beams. Interesting results have also been given by Ramm and Stegmüller (1982) who found that for the 16 node Lagrange with 4x4 quadrature, the buckling value of a cylindrical panel converged only to within 2% of the solution with a 12x12 element (37x37 nodes, 6900 d.o.f.) mesh; they did not report their curved 9-node element results because they were so poor.

Summary of performance. As can be seen, this obstacle course includes problems which compromise the performance of every element except the 9-node γ-element and the DKT-LST. The DKT-LST unfortunately suffers the drawback that it does not have a variational basis. The 4-node SRI element is the next best among these elements, although it exhibits some locking in the pinched cylinder/diaphragm problem.

A confusing result. The senior author has devoted considerable care to the development of methods for controlling spurious modes which are consistent in the sense that the strains for linear displacement fields and rigid body motions are evaluated exactly, which accounts for the terms in addition to $\underset{\sim}{h}$ in the χ projection vector, see Appendix A. However, very good convergence can be obtained in many cases when the additional terms are omitted. Table 3 compares the results for a consistent and inconsistent method of spurious mode control in the hemispherical shell problem; the inconsistent method, in fact, converges faster. The major flaw we have detected in inconsistent methods of stabilization is that it can lead to erroneous stresses in unusually shaped elements where the terms $\underset{\sim}{h}^T\underset{\sim}{x}$ and $\underset{\sim}{h}^T\underset{\sim}{y}$ are large.

Remark 6.2:. The 9-node element solutions which are reported here for the pinched cylinder with diaphragm could be obtained by simply using 2x2 quadrature. When the assembled stiffness matrix obtained with 2 x 2 quadrature is not singular, the γ-method results are almost identical to the results obtained by 2x2 quadrature.

APPENDIX A

The main purpose of this Appendix is to provide details of the 9-node shell element with 2x2 quadrature and the stabilization of the spurious modes by the γ-method. Stabilization procedures of this type were developed for the 4-node plate by Belytschko and Tsay (1983). Results with this γ-element have been reported in Belytschko et al. (1985a) but the consistency of this operator for curved shells was not examined there; formal consistency is equivalent to satisfying the patch test, see Belytschko, et al. (1984a). It will be seen here that once the χ-method is applied to curved elements, certain losses of consistency result, and the stabilization can best be called quasi-consistent. The effect of this is not clear, but as can be seen from the results presented in Section 6 no deleterious effects have been noted. This evidence is however not conclusive since even inconsistent control can perform well, see Table 4.

The degenerated shell element is developed in a manner that closely follows Hughes and Liu (1981). Attention is restricted to the 9-node element. The physical domain of the shell is described by an isoparametric transformation from a reference cube described by coordinates ξ, η, ζ through

$$x_i = \sum_{I=1}^{9} \left(\psi_{I+}(\xi, \eta, \zeta)\, x_{iI+} + \psi_{I-}(\xi, \eta, \zeta)\, x_{iI-}\right) \qquad (A.1)$$

where x_{iI+} and x_{iI-} are the coordinates of the continuum nodes associated with shell node I and x_i are the Cartesian coordinates in the physical space; see Fig. A1. As can be seen from Fig. A1, the nodes labeled I- are below the corresponding shell node I ($\zeta < 0$) while those labeled I+ above the shell node I ($\zeta > 0$).

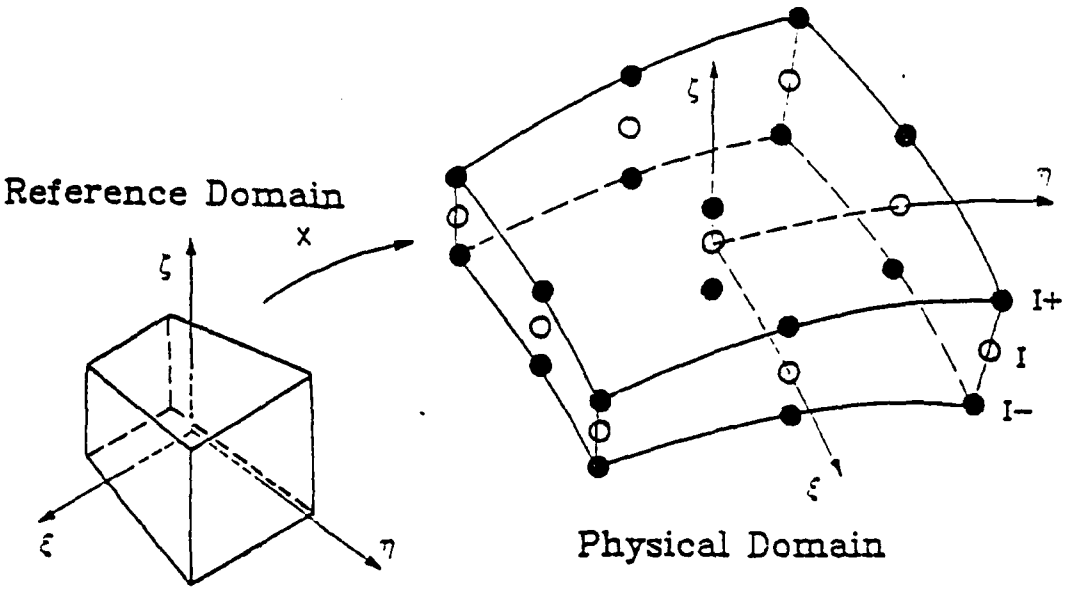

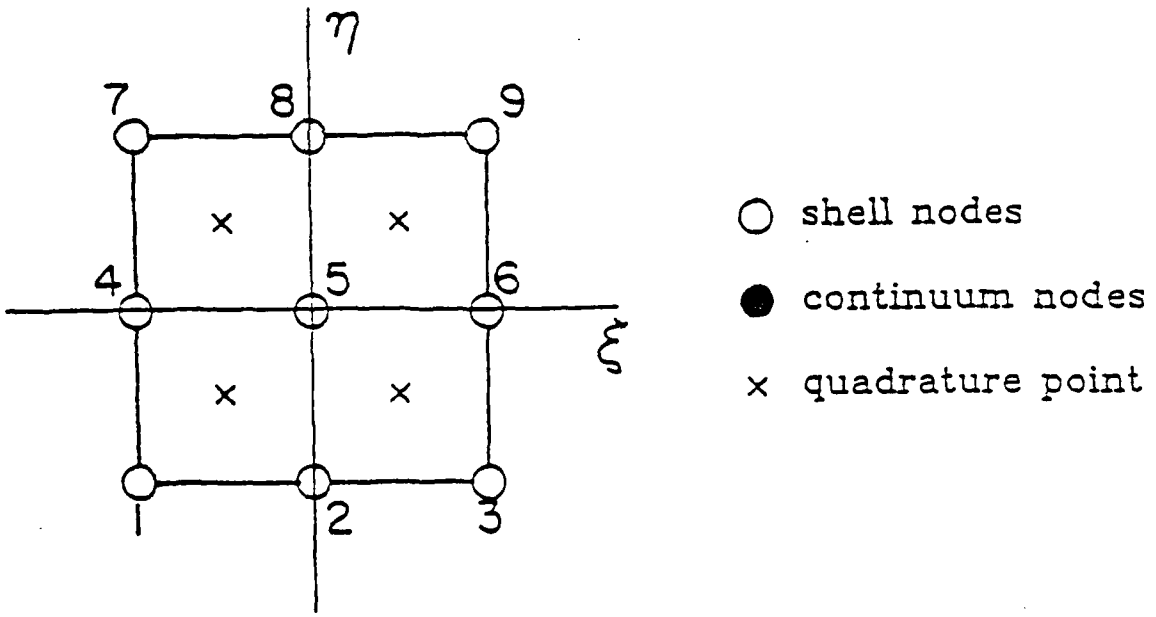

Figure A1. Shell element nomenclature.

The shape functions ψ_I are constructed from the two-dimensional Lagrange interpolant N_I by

$$\psi_{I+} = N_+(\zeta)\, N_I(\xi, \eta) \tag{A.2a}$$

$$\psi_{I-} = N_-(\zeta)\, N_I(\xi, \eta) \tag{A.2b}$$

$$N_+(\zeta) = \tfrac{1}{2}(1 + \zeta) \tag{A.2c}$$

$$N_-(\zeta) = \tfrac{1}{2}(1 - \zeta) \tag{A.2d}$$

$$N_I(\xi, \eta) = \mathcal{L}_J(\xi)\, \mathcal{L}_K(\eta) \qquad I = 3(J - 1) + K \tag{A.2e}$$

$$\mathcal{L}_1(\xi) = \tfrac{1}{2}\xi(\xi - 1) \tag{A.3a}$$

$$\mathcal{L}_2(\xi) = 1 - \xi^2 \tag{A.3b}$$

$$\mathcal{L}_3(\xi) = \tfrac{1}{2}\xi(\xi + 1) \tag{A.3c}$$

The midsurface of the shell is given by (A.1) with $\zeta = 0$, which by means of (A.1-2) can be written

$$x_i = \sum_{I=1}^{9} x_{iI}\, N_I(\xi, \eta) \tag{A.4a}$$

where

$$x_{iI} = \frac{1}{2}\left(x_{iI-} + x_{iI+}\right) \tag{A.4b}$$

The stiffness matrix will be integrated numerically and the points at which the integrand is to be evaluated are called quadrature points. At each quadrature point, a local Cartesian coordinate system $(\hat{x}, \hat{y}, \hat{z})$ is constructed so that the $\hat{x}$, $\hat{y}$ plane is tangent to the midsurface defined by (A.4a) and the $\hat{z}$ coordinate is perpendicular to this plane. If large rotations of the shell are to be treated, this coordinate system can be considered corotational in the sense used by Belytschko and Hsieh (1973) and Belytschko and Marchertas (1974), but this is not of major concern here.

The strain-displacement equations at each quadrature point can be written as

$$\hat{\varepsilon}_{\alpha\beta} = \hat{\varepsilon}^{o}_{\alpha\beta} + \hat{z}\,\hat{\kappa}_{\alpha\beta} \qquad \text{for } \alpha = 1, 2, \quad \beta = 1, 2 \tag{A.5}$$

$$\hat{\varepsilon}_{\alpha z} = \frac{1}{2}\left(\frac{\partial \hat{u}_z}{\partial \hat{x}_\alpha} + \frac{\partial \hat{u}_\alpha}{\partial \hat{x}_z}\right) \qquad \text{for } \alpha = 1,2 \tag{A.6}$$

where

$$\hat{\varepsilon}^{o}_{x} = \frac{\partial \hat{u}_x}{\partial \hat{x}} \tag{A.7a}$$

$$\hat{\varepsilon}^{o}_{y} = \frac{\partial \hat{u}_y}{\partial \hat{y}} \tag{A.7b}$$

$$\hat{\varepsilon}^{o}_{xy} = \frac{1}{2}\left(\frac{\partial \hat{u}_x}{\partial \hat{y}} + \frac{\partial \hat{u}_y}{\partial \hat{x}}\right) \tag{A.7c}$$

$$\hat{\kappa}_x = \frac{\partial \hat{\theta}_y}{\partial \hat{x}} \tag{A.8a}$$

$$\hat{\kappa}_y = -\frac{\partial \hat{\theta}_x}{\partial \hat{y}} \tag{A.8b}$$

$$\hat{\kappa}_{xy} = \frac{1}{2}\left(\frac{\partial \hat{\theta}_y}{\partial \hat{y}} - \frac{\partial \hat{\theta}_x}{\partial \hat{x}}\right) \tag{A.8c}$$

The strain matrix is defined by

$$\hat{\underset{\sim}{\varepsilon}}^T = [\hat{\varepsilon}^{o}_x, \hat{\varepsilon}^{o}_y, 2\hat{\varepsilon}^{o}_{xy}, \hat{\kappa}_x, \hat{\kappa}_y, 2\hat{\kappa}_{xy}, \hat{\varepsilon}_{xz}, \hat{\varepsilon}_{yz}] \tag{A.9}$$

and the $\hat{\underset{\sim}{B}}$ matrix at a quadrature point α gives the strains through

$$\hat{\underset{\sim}{\varepsilon}}^T = \hat{\underset{\sim}{B}}\,(\underset{\sim}{x}_\alpha)\hat{\underset{\sim}{d}} = \sum_{I=1}^{9} \hat{\underset{\sim}{B}}_I(\underset{\sim}{x}_\alpha)\,\hat{\underset{\sim}{d}}_I \tag{A.10}$$

$$\hat{\underset{\sim}{d}}^T = [\hat{\underset{\sim}{d}}_1^T, \hat{\underset{\sim}{d}}_2^T, \ldots . \hat{\underset{\sim}{d}}_9^T] \tag{A.11a}$$

$$\hat{\underset{\sim}{d}}_I^T = [\hat{u}_{xI}, \hat{u}_{yI}, \hat{u}_{zI}, \hat{\phi}_{xI}, \hat{\phi}_{yI}] \tag{A.11b}$$

It should be stressed that the superposed circumflex in the above equations indicates that all components of $\underset{\sim}{\varepsilon}$ and $\underset{\sim}{d}$ are expressed in the corotational coordinate system of point α when evaluating the strain at point α.

For implementation purposes, a transformation $\underset{\sim}{R}$ is defined at each quadrature point so that

$$\hat{\underset{\sim}{d}}_I = \underset{\sim}{R}_I^{\alpha}\, \underset{\sim}{d}_I \tag{A.12}$$

so that

$$\hat{\underset{\sim}{\varepsilon}} = \sum_{I=1}^{9} \hat{\underset{\sim}{B}}_I(\underset{\sim}{x}_{\alpha})\hat{\underset{\sim}{d}}_I \equiv \sum_{I=1}^{9} \hat{\underset{\sim}{B}}_I^{\alpha}\, \underset{\sim}{R}_I^{\alpha}\, \underset{\sim}{d}_I \tag{A.13}$$

where $\underset{\sim}{R}_I^{\alpha}$ is the transformation between the local coordinate system of quadrature point α and the coordinate system of node I. If 5 d.o.f. are used per node, the transformation between α and each node of the shell will be different for a curved element; 5 d.o.f. per node is necessary if singular systems are to be avoided.

The $\hat{\underset{\sim}{B}}$ matrix is given by the component matrices

$$\hat{\underset{\sim}{B}}_I^{\alpha} = \begin{bmatrix} [\hat{B}_m]_I & [0]_{3x3} \\ & [\hat{B}_b]_I \\ [0]_{5x3} & [\hat{B}_s]_I \end{bmatrix} \tag{A.14}$$

$$[\hat{B}_m]_I = \begin{bmatrix} \partial N_I/\partial\hat{x} & 0 \\ 0 & \partial N_I/\partial\hat{y} \\ \partial N_I/\partial\hat{y} & \partial N_I/\partial\hat{x} \end{bmatrix} \tag{A.15}$$

$$[\hat{B}_b]_I = \begin{bmatrix} 0 & 0 & \partial N_I/\partial\hat{x} \\ 0 & -\partial N_I/\partial\hat{y} & 0 \\ 0 & -\partial N_I/\partial\hat{x} & \partial N_I/\partial\hat{y} \end{bmatrix} \tag{A.16}$$

$$[\hat{B}_s]_I = \begin{bmatrix} \partial N_I/\partial\hat{x} & 0 & N_I \\ \partial N_I/\partial\hat{y} & -N_I & 0 \end{bmatrix} \tag{A.17}$$

In uniform reduced quadrature, the element stiffness is given by

$$\underset{\sim}{K}_e = \sum_{\alpha=1}^{4} (\underset{\sim}{R}^{\alpha})^T \hat{\underset{\sim}{B}}^T (\underset{\sim}{x}_\alpha)\, \hat{\underset{\sim}{D}}(\underset{\sim}{x}_\alpha)\, \hat{\underset{\sim}{B}}(\underset{\sim}{x}_\alpha)\, \underset{\sim}{R}^{\alpha}\, J(x_\alpha) \tag{A.18}$$

where $\underset{\sim}{D}$ is the material matrix and J the Jacobian of the mapping between the reference and physical volumes.

Control of Spurious Modes for Plate Bending

The control of spurious modes for the 9 node plate C^0 element has been described by Belytschko, et al. (1984b). However, the method described there is not readily applicable to the curved shell element.

In order to describe the spurious modes and their control, it is convenient to define row vectors $\underset{\sim}{b}_{i\alpha}$, the elements of which are given by

$$b_{1\alpha I} \equiv b_{x\alpha I} = \partial N_I(\underset{\sim}{x}_\alpha)/\partial\hat{x} \tag{A.19a}$$

$$b_{2\alpha I} = b_{y\alpha I} = \partial N_I(\underset{\sim}{x}_\alpha)/\partial \hat{y} \tag{A.19b}$$

and the vectors $\underset{\sim}{s}$ and $\underset{\sim}{h}$ given by

$$\underset{\sim}{s}^T = [1,\ 1,\ 1,\quad 1,\ 1,\ 1,\quad 1,\ 1,\ 1] \tag{A.20}$$

$$\underset{\sim}{h}^T = [+1,\ -1,\ +1,\quad -1,\ 0,\ -1,\quad +1,\ -1,\ +1] \tag{A.21}$$

A single coordinate system is used at all quadrature points of the plate element so $\hat{x}$ is coincident with x, $\hat{y}$ with y. It can be shown that if the quadrature points are $\underset{\sim}{x}_\alpha$, which in the reference plane are given by the four combinations of the coordinates, $\xi = \eta = \pm 3^{-1/2}$ then

$$\underset{\sim}{b}_{i\alpha}^T \underset{\sim}{x}_j = \delta_{ij} \tag{A.22}$$

$$\underset{\sim}{b}_{i\alpha}^T \underset{\sim}{h} = 0 \tag{A.23}$$

$$\underset{\sim}{b}_{i\alpha}^T \underset{\sim}{s} = 0 \tag{A.24}$$

$$\underset{\sim}{N}_\alpha \underset{\sim}{h} = \underset{\sim}{N}(\underset{\sim}{x}_\alpha)\ \underset{\sim}{h} = -\frac{1}{3} \tag{A.25}$$

$$\underset{\sim}{N}_\alpha \underset{\sim}{s} = \underset{\sim}{N}(\underset{\sim}{x}_\alpha)\ \underset{\sim}{s} = 1 \tag{A.26}$$

where $\underset{\sim}{N}$ is the row matrix of shape functions, δ_{ij} is the Kronecker delta, $\underset{\sim}{x}_j$ are the vectors of nodal coordinates of the element. Using (A.22-26), it can easily be verified that the first 3 modes listed in Table A1 are spurious

singular modes of the plate element, which means that

$$\hat{\underset{\sim}{B}}_m(\underset{\sim}{x}_\alpha)\ \hat{\underset{\sim}{d}} = \underset{\sim}{0} \tag{A.27a}$$

and

$$\hat{\underset{\sim}{B}}_s(\underset{\sim}{x}_\alpha)\ \hat{\underset{\sim}{d}} = \underset{\sim}{0} \tag{A.27b}$$

for these nodal displacements which are not rigid body modes. Note that $\underset{\sim}{R}_I^\alpha = \underset{\sim}{I}$ for a plate, and that (A.25-26) are essential in establishing (A.27b).

The control of the spurious modes then consists of defining a projection operator χ which does not destroy the original consistency of the $\underset{\sim}{B}$ matrix, as exhibited by (A.22). Following Belytschko, et al. (1984), the vector χ is expanded in a complete representation of the vector space R^9 through

Table A1

Six Spurious Modes of the 9-Node Element

Mode	$\underset{\sim}{u}_x$	$\underset{\sim}{u}_y$	$\underset{\sim}{u}_z$	$\underset{\sim}{\phi}_x$	$\underset{\sim}{\phi}_y$	$\underset{\sim}{\phi}_z$
1	$\underset{\sim}{0}$	$\underset{\sim}{0}$	$\underset{\sim}{h}$	$\underset{\sim}{0}$	$\underset{\sim}{0}$	$\underset{\sim}{0}$
2	$\underset{\sim}{0}$	$\underset{\sim}{0}$	$\underset{\sim}{0}$	$\underset{\sim}{s} + 3\underset{\sim}{h}$	$\underset{\sim}{0}$	$\underset{\sim}{0}$
3	$\underset{\sim}{0}$	$\underset{\sim}{0}$	$\underset{\sim}{0}$	$\underset{\sim}{0}$	$\underset{\sim}{s} + 3\underset{\sim}{h}$	$\underset{\sim}{0}$
4	$\underset{\sim}{h}$	$\underset{\sim}{0}$	$\underset{\sim}{0}$	$\underset{\sim}{0}$	$\underset{\sim}{0}$	$\underset{\sim}{0}$
5	$\underset{\sim}{0}$	$\underset{\sim}{h}$	$\underset{\sim}{0}$	$\underset{\sim}{0}$	$\underset{\sim}{0}$	$\underset{\sim}{0}$
6	$\underset{\sim}{0}$	$\underset{\sim}{0}$	$\underset{\sim}{0}$	$\underset{\sim}{0}$	$\underset{\sim}{0}$	$\underset{\sim}{s} + 3\underset{\sim}{h}$

$$\chi = \sum_{\alpha=1}^{4} (a_{1\alpha}\, \underset{\sim}{b}_{1\alpha} + a_{2\alpha}\, \underset{\sim}{b}_{2\alpha}) + a_9\, \underset{\sim}{h} + a_{10}\, \underset{\sim}{s} \qquad \text{(A.28)}$$

Ten vectors are needed because $\underset{\sim}{b}_{i\alpha}$ are not all linearly independent. Linear consistency then requires that

$$\chi^T(c_o\, \underset{\sim}{s} + c_1\, \underset{\sim}{x} + c_2\, \underset{\sim}{y}) = 0 \qquad \text{for all } c_i \qquad \text{(A.29a)}$$

Substituting (A.28) into (A.29a) and using (A.22-24) yields

$$\begin{aligned} c_o(a_{10}\, \underset{\sim}{s}^T\, \underset{\sim}{s}) + c_1\, (a_9\, \underset{\sim}{h}^T\, \underset{\sim}{x} + a_{10}\, \underset{\sim}{s}^T\, \underset{\sim}{x} + \sum_{\alpha=1}^{4} a_{1\alpha}) \\ + c_2\, (a_9\, \underset{\sim}{h}^T\, \underset{\sim}{y} + a_{10}\, \underset{\sim}{s}^T\, \underset{\sim}{y} + \sum_{\alpha=1}^{4} a_{2\alpha}) = 0 \end{aligned} \qquad \text{(A.29b)}$$

Since the above must hold for all c_i, it follows that $a_{10} = 0$ and only 2 conditions need be satisfied by $a_{i\alpha}$. Thus a large variety of options are available in the consistent control of the spurious modes. In Belytschko, et al. (1984), it was chosen to let

$$a_{1\alpha} = -\frac{1}{4}\, a_9\, \underset{\sim}{h}^T\, \underset{\sim}{x} \qquad a_{2\alpha} = -\frac{1}{4}\, a_9\, \underset{\sim}{h}^T\, \underset{\sim}{y} \qquad \alpha = 1 \text{ to } 4 \qquad \text{(A.30)}$$

However, this approach is not adaptable to the shell problem, as will become clear shortly.

The approach that is therefore taken is to define a projection operator χ_β at each quadrature point. Equation (A.29) must hold for <u>each</u> χ_β and this is accomplished by letting

$$a_{i\alpha} = \begin{cases} 0 & \text{if} \quad \alpha \neq \beta \\ -a_9 \, \underset{\sim}{h}^T \underset{\sim}{x}_i & \text{if} \quad \alpha = \beta \end{cases} \tag{A.31}$$

Hence

$$\chi_\beta = \underset{\sim}{h} - (\underset{\sim}{h}^T \underset{\sim}{x}) \, \underset{\sim}{b}_{x\beta} - (\underset{\sim}{h}^T \underset{\sim}{y}) \, \underset{\sim}{b}_{y\beta} \tag{A.32}$$

The common constant a_9 has been omitted.

In this scheme, 12 generalized strains (in contrast to 3 in the original scheme) are then defined by

$$\begin{aligned} q_\beta^{(w)} &= \chi_\beta^T \, \underset{\sim}{u}_z \\ q_{x\beta}^{(\phi)} &= \chi_\beta^T \, \underset{\sim}{\phi}_x \qquad\qquad \beta = 1 \text{ to } 4 \\ q_{y\beta}^{(\phi)} &= \chi_\beta^T \, \underset{\sim}{\phi}_y \end{aligned} \tag{A.33}$$

where β identifies the quadrature point.

Spurious Mode Control for 9 Node Shell The six modes which are to be controlled are listed in Table A1. The form of a spurious mode projection has been presented in Belytschko, et al. (1985) but a careful examination of its consistency and limitations is still not available. We will attempt to partially remedy these shortcomings here.

The issues of consistency (and the related issues of patch tests) for shells still appear unresolved. While the requirement that an element be

strain-free in rigid body motion is quite clear, the additional consistency requirements associated with linear fields are more difficult to formulate in a curved element.

For this reason, we have taken advantage of the relationship between the shell and continuum elements (see Fig. A1) to develop as consistent an operator as possible. As in the new plate version of the spurious mode projection just described, the projection operator is defined at each quadrature point α, and denoted by χ_α. Consistency then requires that

$$\chi_\alpha^T \left(c_0 \underset{\sim}{s} + \sum_{j=1}^{3} c_j \hat{\underset{\sim}{x}}_j\right) = 0 \quad \text{for all } c_j \tag{A.34}$$

where

$$\chi_\alpha = a_9 \underset{\sim}{h} + a_{x\alpha} \hat{\underset{\sim}{b}}_{x\alpha} + a_{y\alpha} \hat{\underset{\sim}{b}}_{y\alpha} \tag{A.35}$$

Note that we have immediately dropped the $\hat{\underset{\sim}{b}}_{i\beta}$ matrices associated with quadrature points other than α, as in Eq. (A.31), and a_{10}, which must obviously vanish as before. Furthermore, in contrast to (A.29), consistency is now required with respect to fields linear in $\hat{z}$ (that is $\hat{x}_3$).

We now define

$$\hat{\beta}_{i\alpha I\pm} = \frac{\partial \psi_{I\pm}(\underset{\sim}{x}_\alpha)}{\partial \hat{x}_i} \qquad \begin{matrix} I = 1 \text{ to } 9 \\ i = 1 \text{ to } 3 \end{matrix} \tag{A.36}$$

that is, $\hat{\underset{\sim}{\beta}}_{i\alpha}$ are the derivatives of the continuum node shape functions. By consistency of the original continuum shape functions

$$\hat{\underset{\sim}{\beta}}_{i\alpha}^{T}\,\hat{\underset{\sim}{x}}_j = \sum_{I=1}^{9}\left(\hat{\beta}_{i\alpha I+}\,\hat{x}_{jI+} + \hat{\beta}_{i\alpha I-}\,\hat{x}_{jI-}\right) = \delta_{ij} \qquad i,\ j = 1 \text{ to } 3 \tag{A.37}$$

where the sum is over the continuum nodes and $\underset{\sim}{r}_j = (\underset{\sim}{x}_{j-},\ \underset{\sim}{x}_{j+})$, which are the coordinates of the continuum nodes.

Using (A.2), it can be seen that

$$\frac{\partial \psi_{I+}(\xi,\eta,0)}{\partial \hat{x}_i} = \frac{\partial N_+}{\partial \hat{x}_i} N_I + N_+ \frac{\partial N_I}{\partial \hat{x}_i} = \frac{1}{2}\frac{\partial N_I}{\partial \hat{x}_i} \qquad \text{for } i = 1,\ 2 \tag{A.38}$$

A similar expression applies to the nodes below the midplane, I-. It has been assumed that ζ is normal to the $(\hat{x},\ \hat{y})$ plane so that $\partial N_+/\partial \hat{x}_i = 0$. Since this cannot hold exactly the approximate equality is used in (A.38).

Using (A.38) and (A.4b), it follows that for i = 1, 2; j = 1 to 3

$$\begin{aligned}\hat{\underset{\sim}{\beta}}_{i\beta}^{T}\,\hat{\underset{\sim}{r}}_j &= \sum_{I=1}^{9}\frac{\partial N_I}{\partial \hat{x}_i}\left[\frac{1}{2}\left(\hat{x}_{jI-} + \hat{x}_{jI+}\right)\right] \\ &= \sum_{I=1}^{9}\frac{\partial N_I}{\partial \hat{x}_i}\,\hat{x}_{jI}\end{aligned} \tag{A.39}$$

Hence using (A.19), (A.37) and (A.39)

$$\hat{\underset{\sim}{b}}_{i\alpha}^{T}\,\hat{\underset{\sim}{x}}_j = \delta_{ij} \qquad \text{for } i = 1,\ 2 \qquad j = 1 \text{ to } 3 \tag{A.40}$$

Employing (A.34-35) with (A.40), it follows that the requirements for consistency are

$$\underset{\sim}{h}^T \hat{\underset{\sim}{x}} + a_{x\alpha} = 0 \qquad \text{(A.41a)}$$

$$\underset{\sim}{h}^T \hat{\underset{\sim}{y}} + a_{y\alpha} = 0 \qquad \text{(A.41b)}$$

$$\underset{\sim}{h}^T \hat{\underset{\sim}{z}} = 0 \qquad \text{(A.41c)}$$

Equations (A.41a-b) can be satisfied exactly as in the development of the flat plate operator, (A.32), so that the projection operator at each point becomes

$$\gamma_\alpha = \underset{\sim}{h} - (\underset{\sim}{h}^T \hat{\underset{\sim}{x}})\, \hat{\underset{\sim}{b}}_{x\alpha} - (\underset{\sim}{h}^T \hat{\underset{\sim}{y}})\, \hat{\underset{\sim}{b}}_{y\beta} \qquad \text{(A.42)}$$

However, (A.41c) <u>cannot</u> be satisfied and there is no latitude with which to attack it, so that the method as described here must violate consistency whenever $\underset{\sim}{h}^T \hat{\underset{\sim}{z}} \neq 0$.

The control of the spurious modes is then accomplished by defining 5 additional generalized strains at each of the four laminar quadrature points through

$$g_{i\alpha}^{(m)} = \hat{\gamma}_\alpha^T \hat{\underset{\sim}{u}}_i \qquad i = 1, 2$$

$$g_{3\alpha}^{(w)} = \hat{\gamma}_\alpha^T \hat{\underset{\sim}{u}}_z \qquad \text{(A.43)}$$

$$g_{i\alpha}^{(\phi)} = \hat{\gamma}_\alpha \hat{\phi}_i \qquad i = 1, 2$$

The first two generalized strains control the spurious membrane modes, the next three control the bending modes.

The stiffness matrix of the element is then given by adding the effects of the stabilization to $\underset{\sim}{K}_e$ see (A.18), which gives

$$\underset{\sim}{K}_e = \sum_{\alpha=1}^{4} (\underset{\sim}{R}^{\alpha})^T (\hat{B}^T(\underset{\sim}{x}_\alpha)\ \hat{\underset{\sim}{D}}(\underset{\sim}{x}_\alpha)\ \hat{\underset{\sim}{B}}(\underset{\sim}{x}_\alpha)\ J(\underset{\sim}{x}_\alpha) + (\underset{\sim}{\Gamma}^{\alpha})^T \underset{\sim}{\Gamma}^{\alpha})\ \underset{\sim}{R}^{\alpha} \qquad \text{(A. 44)}$$

where J is the Jacobian and $\underset{\sim}{\Gamma}^{\alpha}$ is a diagonal matrix consisting of blocks $\underset{\sim}{\Gamma}^{\alpha}_I$ given by

$$\underset{\sim}{\Gamma}^{\alpha}_I = \begin{bmatrix} r_m \gamma_{\alpha I} & & & & \\ & r_m \gamma_{\alpha I} & & & \text{zeroes} \\ & & r_w \gamma_{\alpha I} & & \\ & \text{zeroes} & & r_\theta \gamma_{\alpha I} & \\ & & & & r_\theta \gamma_{\alpha I} \end{bmatrix}$$

(A.45)

It has been shown by Belytschko, et al. (1984) via the Hu-Washizu principle that the γ-method stabilization is equivalent to recovering that portion of the diagonal terms of the stiffness matrix which has been lost by reduced quadrature. Specific equations for the r-parameters have been given by Belytschko, et al. (1985a). One important observation on the choice of the r-parameters is that while r_θ and r_m can be chosen so that the fully integrated stiffness is recovered, r_w must be scaled down to about 0.1; otherwise, the element locks.

APPENDIX B

AN EQUIVALENT MIXED ELEMENT

We show here a construction of the strain and stress fields such that the resulting 9-node mixed element is formally equivalent to the 9-node 2x2 quadrature displacement element. The demonstration is limited to the membrane portion of the 9-node element, but it can easily be extended to the complete shell element. The demonstration is the spirit of the Malkus-Hughes (1978) equivalence theorem but offers the interesting feature that by using Dirac functions for the stress interpolants, the demonstration provides an equivalence with the exactly integrated mixed element. We assume that the material properties of the element are constant.

The essential ingredient in the demonstration of the equivalence is the construction of the interpolation functions for the strains and stresses which are used in the Hu-Washizu functional. For conceptual simplicity, it is important to choose the functions so that the orthogonality condition (3.8) is met. This is accomplished as follows.

The element is subdivided into 4 subdomains Ω_1 to Ω_4 so that Ω_I contains integration point x_I and no two subdomains Ω_I overlap, i.e. $\Omega_I \cap \Omega_J = 0$ if $I \neq J$; see Fig. B1 for the subdivision.

We then define Heaviside functions by

$$H_I(\underset{\sim}{x}) = \begin{cases} 1 & \text{if } \underset{\sim}{x} \text{ is in } \Omega_I \\ 0 & \text{if } \underset{\sim}{x} \text{ is not in } \Omega_I \end{cases} \tag{B.1}$$

The Dirac delta function is denoted by $\delta(\underset{\sim}{x} - \underset{\sim}{x}_I)$. Note that

$$\int_{\Omega} H_I(x)\ \delta(x - x_J)d\Omega = I_{IJ} \tag{B.2}$$

where I_{IJ} are the components of the unit matrix $\underset{\sim}{I}$.

The strains and stresses are now interpolated as follows (see Fig. B1 for an illustration of the shape functions)

$$\begin{Bmatrix} \varepsilon_x \\ \varepsilon_y \\ \varepsilon_{xy} \end{Bmatrix} = [\underset{\sim}{E}_1, \underset{\sim}{E}_2, \underset{\sim}{E}_2, \underset{\sim}{E}_4] \begin{Bmatrix} \underset{\sim}{e}_1 \\ \underset{\sim}{e}_2 \\ \underset{\sim}{e}_3 \\ \underset{\sim}{e}_4 \end{Bmatrix} \tag{B.3}$$

$$\begin{Bmatrix} \sigma_x \\ \sigma_y \\ \sigma_{xy} \end{Bmatrix} = [\underset{\sim}{S}_1, \underset{\sim}{S}_2, \underset{\sim}{S}_3, \underset{\sim}{S}_4] \begin{Bmatrix} \underset{\sim}{s}_1 \\ \underset{\sim}{s}_2 \\ \underset{\sim}{s}_3 \\ \underset{\sim}{s}_4 \end{Bmatrix} \tag{B.4}$$

where

$$\underset{\sim}{E}_I = H_I(\underset{\sim}{x})\ \underset{\sim}{I}_{3x3} \equiv \begin{bmatrix} H_I & 0 & 0 \\ 0 & H_I & 0 \\ 0 & 0 & H_I \end{bmatrix} \tag{B.5}$$

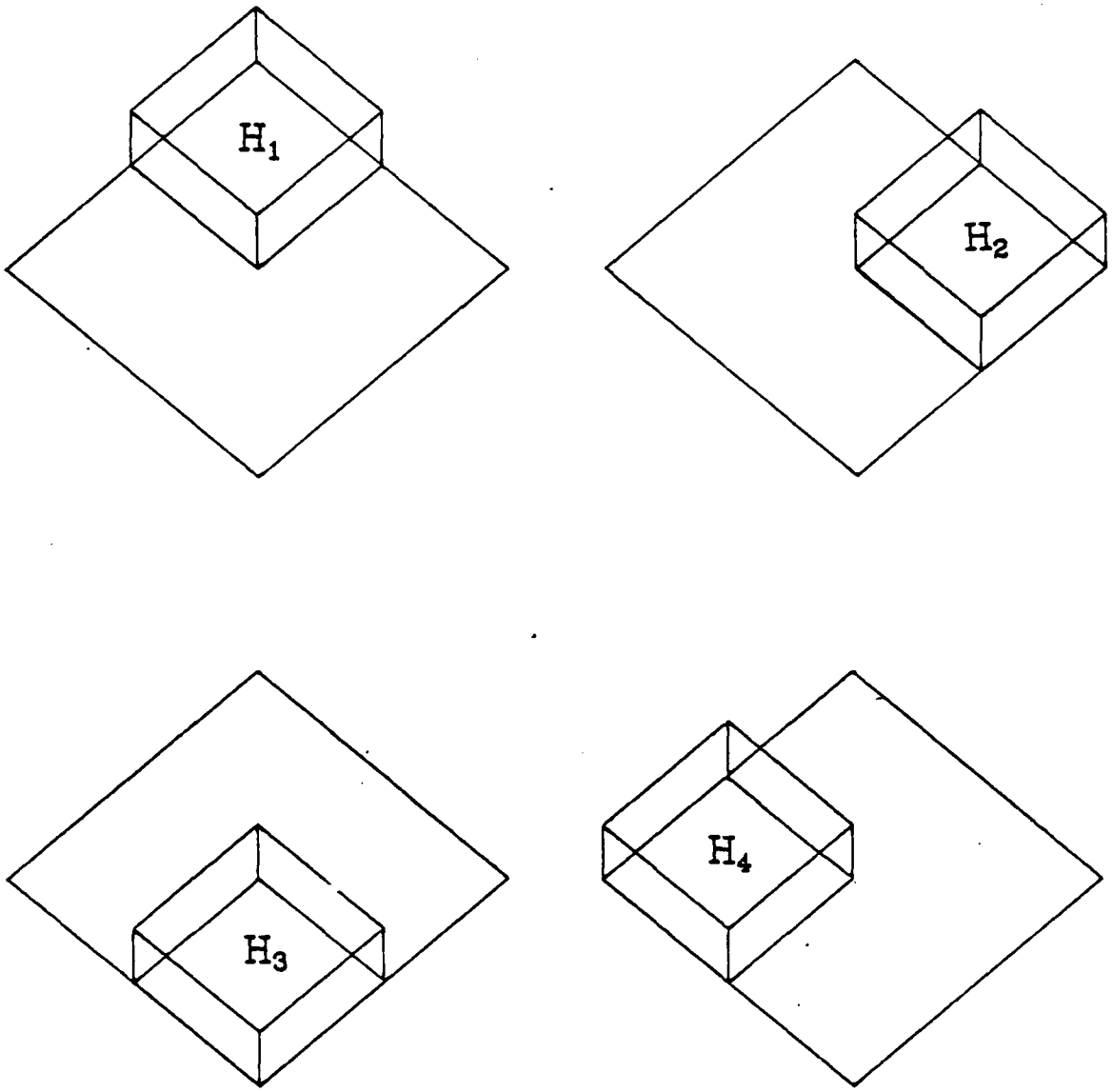

Figure B1. Shape functions for mixed method equivalent to 2x2 quadrature.

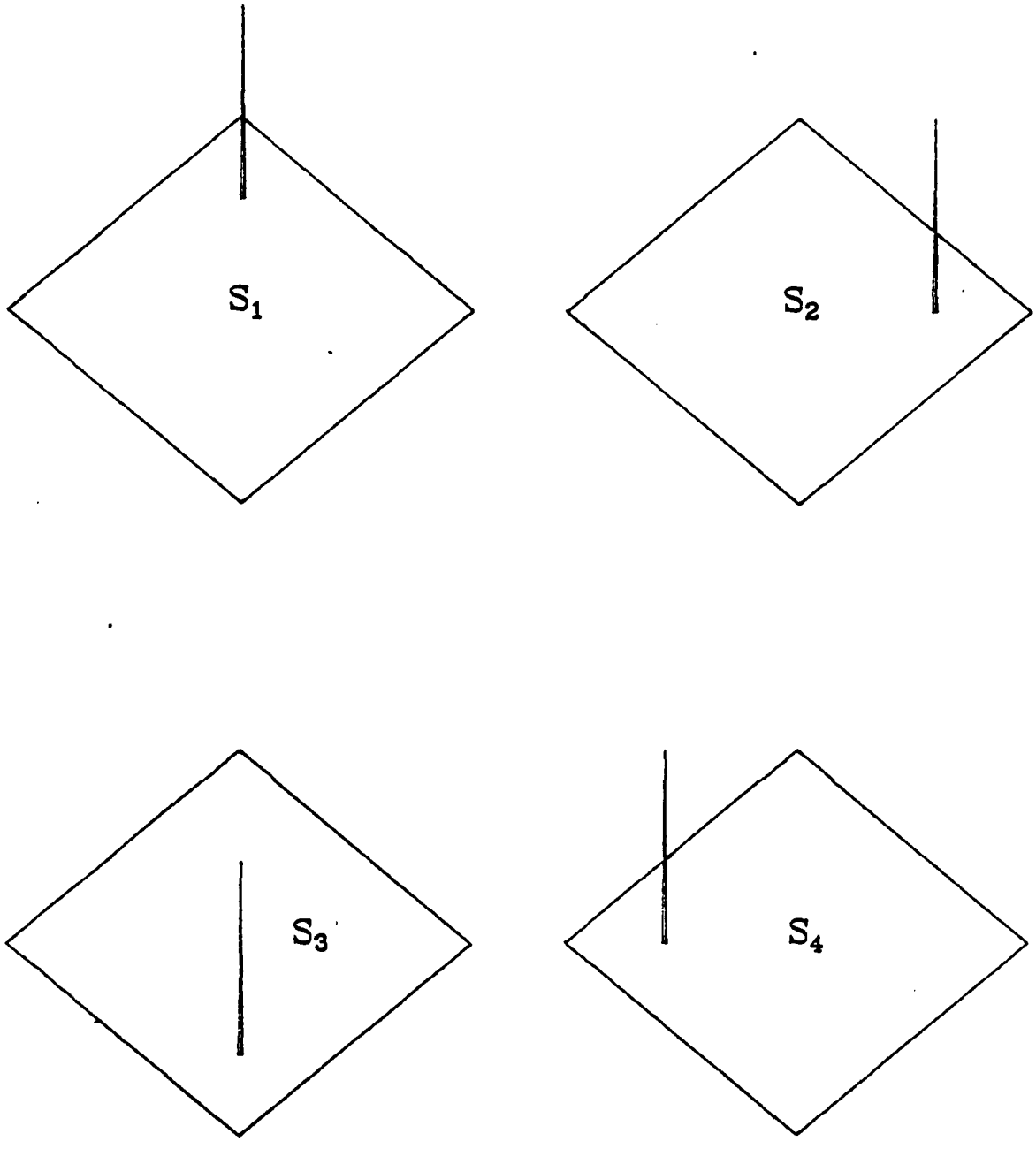

Figure B1. Shape functions for mixed method equivalent to 2x2 quadrature.

$$\underset{\sim}{S}_I = \delta(\underset{\sim}{x} - \underset{\sim}{x}_I)\underset{\sim}{I}_{3x3} = \begin{bmatrix} \delta(\underset{\sim}{x}-\underset{\sim}{x}_I) & 0 & 0 \\ 0 & \delta(\underset{\sim}{x}-\underset{\sim}{x}_I) & 0 \\ 0 & 0 & \delta(\underset{\sim}{x}-\underset{\sim}{x}_I) \end{bmatrix} \qquad (B.6)$$

Let

$$\underset{\sim}{e}_I = \begin{Bmatrix} e_{xI} \\ e_{yI} \\ e_{xyI} \end{Bmatrix} \quad \underset{\sim}{s}_I = \begin{Bmatrix} s_{xI} \\ s_{yI} \\ s_{xyI} \end{Bmatrix} \qquad (B.7a)$$

$$\underset{\sim}{e} = \begin{bmatrix} \underset{\sim}{e}_1 \\ \underset{\sim}{e}_2 \\ \underset{\sim}{e}_3 \\ \underset{\sim}{e}_4 \end{bmatrix} \quad \underset{\sim}{s} = \begin{bmatrix} \underset{\sim}{s}_1 \\ \underset{\sim}{s}_2 \\ \underset{\sim}{s}_3 \\ \underset{\sim}{s}_4 \end{bmatrix} \qquad (B.7b)$$

It is easily verified from (3.8a) and (B.2) that

$$\overline{\underset{\sim}{E}}_{IJ} = \int_\Omega \underset{\sim}{S}_I^T \underset{\sim}{E}_J \, d\Omega = I_{IJ} \, \underset{\sim}{I}_{(3x3)}$$

$$\text{or} \quad \overline{\underset{\sim}{E}} = \underset{\sim}{I}_{(12x12)} \qquad (B.8)$$

From (3.8b) and (B.6) it follows that

$$\overline{\underset{\sim}{B}} = \int \underset{\sim}{S}^T \underset{\sim}{B}\, d\Omega = \begin{bmatrix} \underset{\sim}{B}(\underset{\sim}{x}_1) \\ \underset{\sim}{B}(\underset{\sim}{x}_2) \\ \underset{\sim}{B}(\underset{\sim}{x}_3) \\ \underset{\sim}{B}(\underset{\sim}{x}_4) \end{bmatrix} \tag{B.9}$$

from (3.6c) and (B.5) that

$$\overline{\underset{\sim}{D}} = \begin{bmatrix} A_1\underset{\sim}{D} & \underset{\sim}{0} & \underset{\sim}{0} & \underset{\sim}{0} \\ & A_2\underset{\sim}{D} & \underset{\sim}{0} & \underset{\sim}{0} \\ \text{symmetric} & & A_3\underset{\sim}{D} & \underset{\sim}{0} \\ & & & A_4\underset{\sim}{D} \end{bmatrix} \tag{B.10}$$

where A_I are the areas of the subdomains Ω_I.

From (3.12), (B.9) and (B.10) it follows that

$$\underset{\sim}{K}_e = \overline{\underset{\sim}{B}}^T \overline{\underset{\sim}{D}}\, \overline{\underset{\sim}{B}} = \sum_{I=1}^{4} A_I\, \underset{\sim}{B}^T(\underset{\sim}{x}_I)\, \underset{\sim}{D}\, \underset{\sim}{B}\, (\underset{\sim}{x}_I) \tag{B.11}$$

which is analogous to the form of the numerically integrated displacement stiffness except that A_I replaces the determinant of the Jacobian $J_I = J(\underset{\sim}{x}_I)$; see (A.18). Note that the weights for 2x2 Gauss quadrature are all unity. However, the completion of the proof requires that it be shown that Ω_I can be constructed so that $J_I = A_I$.

To show that for an arbitrary isoparametric quadratic Lagrange element the partition of Ω into Ω_I such that $A_I = J_I$ is possible, we observe that

$$J(\xi, \eta) = \det \begin{vmatrix} x_{,\xi} & x_{,\eta} \\ y_{,\xi} & y_{,\eta} \end{vmatrix} \tag{B.12a}$$

is a cubic function of both ξ and η. Thus 2x2 quadrature evaluates the area of the element exactly

$$A = \int_{-1}^{1}\int_{-1}^{1} J(\xi, \eta)\, d\xi\, d\eta = \sum_{I=1}^{4} J_I \qquad (B.12b)$$

The above equation indicates that letting $A_I = J_I$ we have $\sum_I A_I = A$. The partition of Ω into four such nonoverlapping Ω_I should be possible, since the only restriction is that each integration point $\underset{\sim}{x}_I$ falls within Ω_I.

It is also of interest to write the intermediate equations, namely, the counterparts of (3.10). Using (B.7-10) these can be written as

$$\underset{\sim}{e}_I = \underset{\sim}{B}(\underset{\sim}{x}_I)\, \underset{\sim}{d} \qquad (B.13a)$$

$$\underset{\sim}{s}_I = A_I\, \underset{\sim}{D}\, \underset{\sim}{e}_I \qquad (B.13b)$$

$$\underset{\sim}{f} = \overline{\underset{\sim}{B}}^T\, \underset{\sim}{s} = \sum_{I=1}^{n_E} \underset{\sim}{B}^T(\underset{\sim}{x}_I)\, \underset{\sim}{s}_I \qquad (B.13c)$$

The above clearly brings out the structure of this mixed method. The strain parameters are simply the strains at the quadrature points, the stresses are only modified by the areas (Jacobians).

An almost equivalent mixed method can be constructed by letting

$$\underset{\sim}{S}_I = H_I(\underset{\sim}{x})\underset{\sim}{I}_{3x3} \qquad (B.14)$$

Then $\overline{\underset{\sim}{E}}$ is block-diagonal with the blocks given by

$$\overline{\underset{\sim}{E}}_{II} = A_I \, \underset{\sim}{I}_{(3x3)} \tag{B.15}$$

and (B.9) is then replaced by

$$\overline{\underset{\sim}{E}}^{-1} \, \overline{\underset{\sim}{B}} = \int_{\Omega} \underset{\sim}{S}^T \, \underset{\sim}{B} \, d\Omega = \begin{bmatrix} \underset{\sim}{B}(\bar{\underset{\sim}{x}}_1) \\ \underset{\sim}{B}(\bar{\underset{\sim}{x}}_2) \\ \underset{\sim}{B}(\bar{\underset{\sim}{x}}_3) \\ \underset{\sim}{B}(\bar{\underset{\sim}{x}}_4) \end{bmatrix} \tag{B.16}$$

where by the mean value theorem, $\bar{x}_I$ is some point in Ω_I (usually not the Gauss quadrature point). Equations analogous to (B.11) and (B.13) can be developed for this construction.

It is not clear whether this construction falls within the scope of the convergence proof given by Oden and Reddy (1974). However, the use of Dirac delta functions makes this method a hybrid of collocation and Galerkin methods, for which convergence theory should be feasible.

APPENDIX C

C.1 Impulsively Loaded Cylindrical Panel

This problem is defined in Fig. C.1 and Table C.2. The Ends of the panel are simply-supported, while the side boundaries are fixed. Both material and geometric nonlinearities were considered. The load was applied by prescribing the initial velocity given in Fig. C.2 to the nodes in the region loaded by the explosive. Figure C.3 shows an undeformed and deformed mesh. Table C.2 compares the results obtained for various meshes to an experimental result. It can be seen that convergence to the experimental value is relatively slow. The reason for this however, is not the accuracy of the element, but tne extreme localization of deformation which occurs due to the formation of plastic hinges.

C.2 Collapse of a Hollow Column

Figure C.4 shows the simulation of a hollow column loaded axially. The time history of the load and material and geometric properties may be found in Fig. 3 and Table 1 of Kennedy and Belytschko (1982) where results obtained with a 4-node quadrilateral element using one-point quadrature and hourglass control are also given. The results obtained with this element compare well with those obtained for the quadrilateral, except the model is somewhat stiffer. Note the severe change n cross-section which accompanies buckling.

TABLE C.1

Material and Geometric Constants for Impulsively Loaded Cylindrical Panel

Young's modulus	$E = 10.5 \times 10^6$
Density	$\rho = 2.5 \times 10^4$ lb-sec^2/in^4
Poisson's ratio	$\nu = 0.33$
Yield stress	$\sigma = 44000.$ psi
Plastic modulus	$E_p = 0.$ psi
Impulse over R_I	5650 in/sec

TABLE C.2

Final Displacements of the Cylindrical Panel
for Various Meshes with Ilyushin Yield Condition

Mesh Half-panel	Displacement at y = 6.28	Displacement at y = 9.42	CPU time IBM 3033
6 x 16	0.917	0.401	83
8 x 16	1.043	0.448	138
10 x 20	1.081	0.462	162
12 x 24	1.124	0.473	291
16 x 32	1.183	0.530	670
experimental [48]	1.28	0.70	

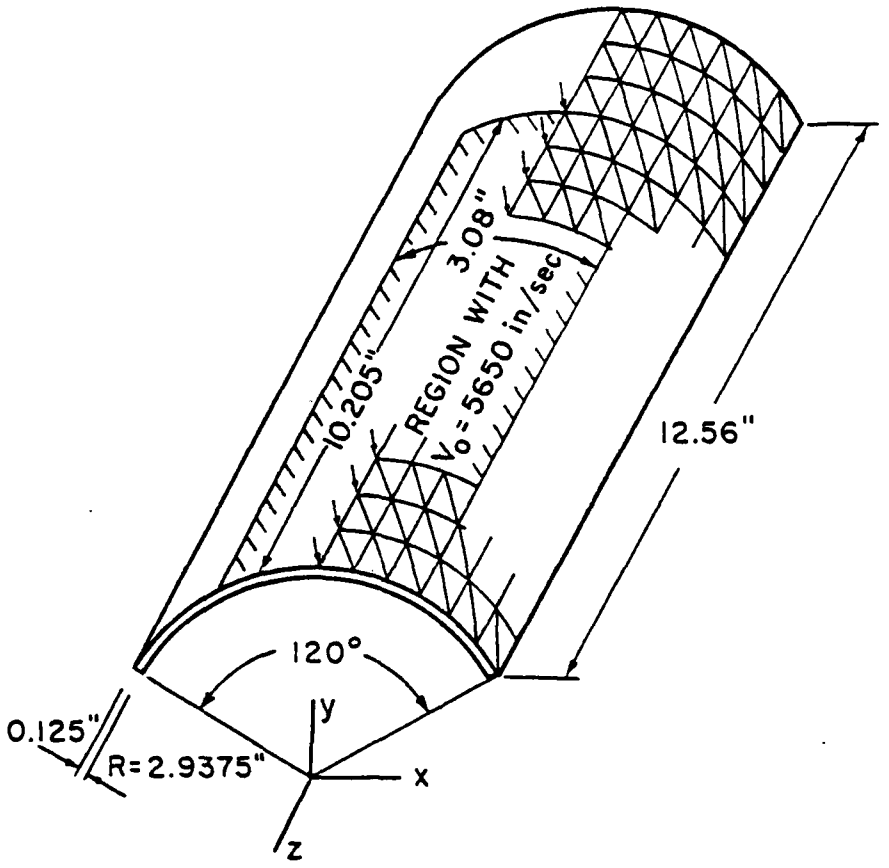

ELASTIC-PLASTIC CYLINDER PROBLEM

Figure C.1

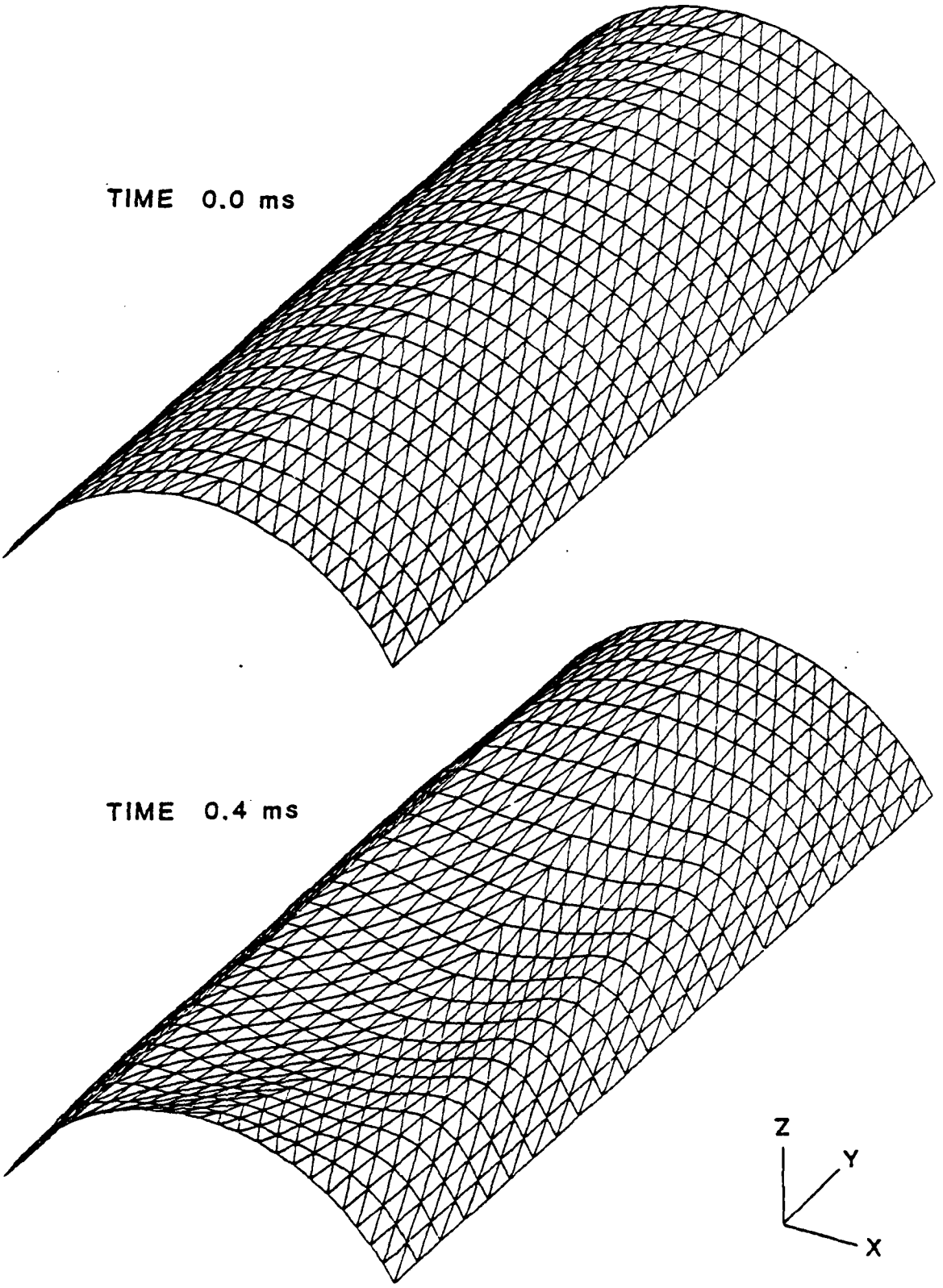

Figure C.2

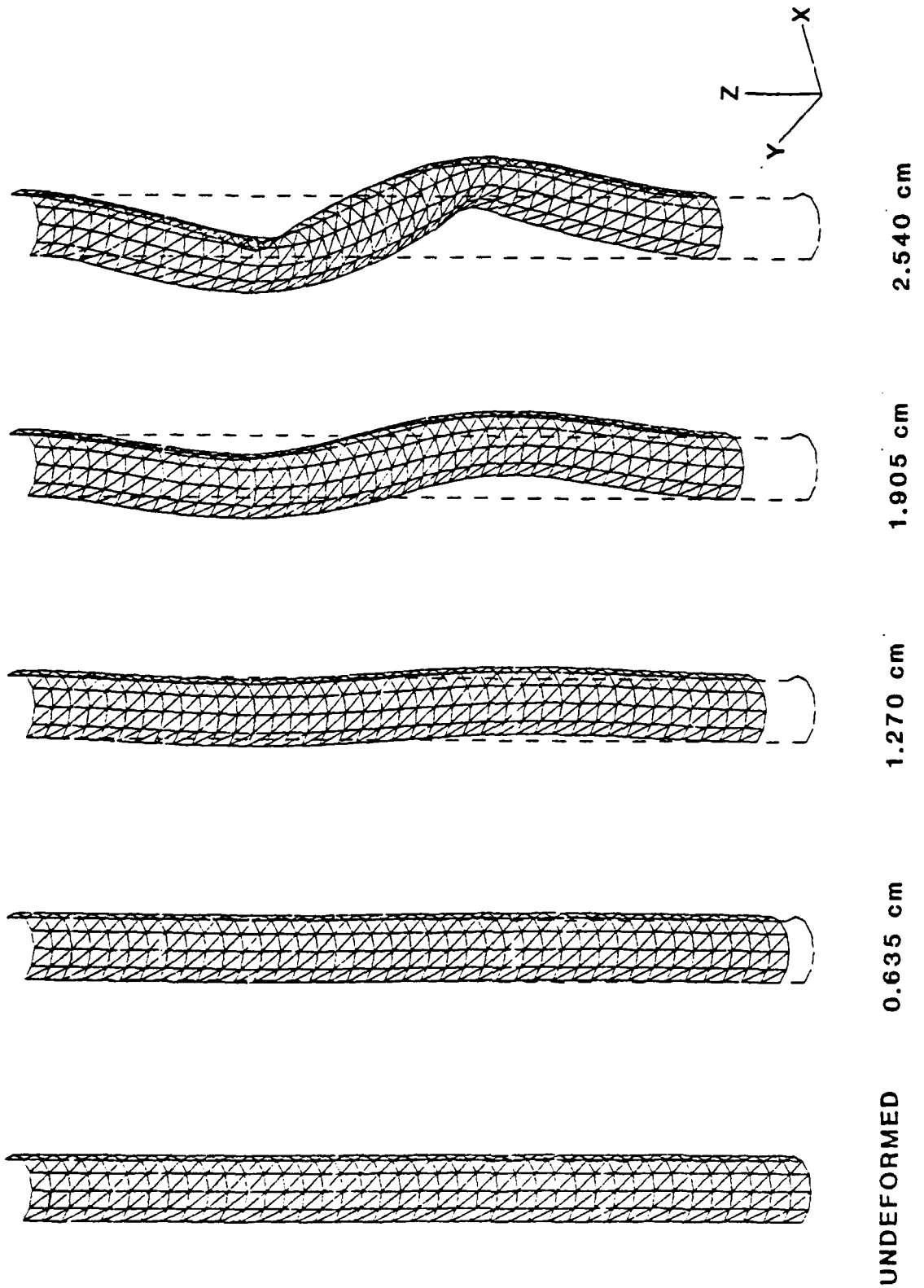

Figure C.3

REFERENCES

D.J. Allman (1982), "Improved Finite Element Models for the Large Displacement Bending and Post Buckling analysis of Thin Plates," Int. J. Solids Struct., 9, 18, pp. 737-762.

J.H. Argyris (1965), "Continua and Discontinua," Proceedings of the First Conference on Matrix Methods in Structural Mechanics, Wright Patterson Air Force Base, Ohio, pp. 26-28.

J.H. Argyris and D. Scharpf (1968), "The SHEBA Family of Shell Elements for the Matrix Displacement Method," The Aeronautical Journal, pp. 873-883.

D.N. Arnold (1981), "Discretization by Finite Elements of a Model Parameter Dependent Problem," Numer. Math., 37, pp. 405-421.

D.G. Ashwell and A.B. Sabir (1971), "Limitations of Certain Curved Finite Elements When Applied to Arches," Int. J. Mech. Sci., 13, pp. 133-139.

D.G. Ashwell (1976), "Strain Elements, with Applications to Arches, Rings and Cylindrical Shells," Finite Elements for Thin Shells and Curved Members, John Wiley & Sons.

J.L. Batoz (1982), "An Explicit Formulation for an Efficient Triangular Plate-Bending Element," Int. J. Num. Meth. Eng., 18, pp. 1077-1089.

T. Belytschko and B.J. Hsieh (1973), "Nonlinear Transient Finite Element Analysis with Convected Coordinates," Int. J. Num. Meth. Eng., 3, pp. 255-272.

T. Belytschko and A.H. Marchertas (1974), "Nonlinear Finite Element Methods for Plates and Its Application to Dynamic Response of Reactor Fuel Subassemblies," ASME Journal of Pressure Vessel Technology, pp. 251-257.

T. Belytschko and L.W. Glaum (1979), "Application of High Order Corotational Stretch Theory to Nonlinear Finite Element Analysis," Computers and Structures, 10, pp. 175-182.

T. Belytschko, J.I. Lin C.S. Tsay (1984), "Explicit Algorithms for the Nonlinear Dynamics of Shells,"Computer Methods in Applied Mechanics and Engineering, 42, pp. 225-251.

J.M. Kennedy and T. Belytschko (1982), "Buckling and Post-buckling Behavior of the ACS Support Columns," Nuclear Engineering and Design, 75, pp. 323-342.

T. Belytschko and C.S. Tsay (1983), "A Stabilization Procedure for the Quadrilateral Plate Element with One-Point Quadrature," Int. Journal for Numerical Methods in Engineering, 19, pp. 405-420.

T. Belytschko, J.S.-J. Ong, W.K. Liu and J.M. Kennedy (1984a), "Hourglass Control in Linear and Nonlinear Problems, Comp. Meth. in Appl. Mech. and Engrg., 43, pp. 251-276.

T. Belytschko, W.K. Liu and J.S-J. Ong (1984b), "A Consistent Control of Spurious Singular Modes in the 9-Node Lagrange Element for the Laplace and Mindlin Plate Equations," Comp. Meth. in Appl. Mech. and Engrg., 44, pp. 269-295.

T. Belytschko, H. Stolarski and N. Carpenter (1984c), "A C^0 Triangular Plate Element with One-Point Quadrature," Int. J. Num. Meth. Eng., 20, pp. 787-802.
T. Belytschko, W.K. Liu, J.S-J. Ong and D. Lam (1985a), "Implementation and Application of a 9-Node Lagrange Shell Element with Spurious Mode Control," Computers and Structures, to appear.

T. Belytschko, H. Stolarski and B.L. Wong (1985b), "A Strain Projection Approach to the Cure of Membrane Locking," Computers and Structures, to appear.

N. Carpenter, H. Stolarski and T. Belytschko (1985), "A Flat Triangular-Shell Element with Improved Membrane Interpolation," Communications in Applied Numerical Methods, to appear.

G.R. Cowper, G.M. Lindberg and M.D. Olson (1970), "A Shallow Shell Finite Element of Triangular Shape," Int. J. Solids Struct., 6, p. 1133.

D.J. Dawe (1974), "Curved Finite Elements for the Analysis of Shallow and Deep Arches," Comp. and Structures, 4, pp. 559-580.

W.P. Doherty, E.L. Wilson and R.L. Taylor (1969), "Stress Analysis of Axisymmetric Solids Utilizing Higher Order Quadrilateral Finite Elements," Structural Engineering Laboratory, University of California, Berkeley.

E.N. Dvorkin and K.J. Bathe (1984), "A Continuum Mechanics Based Four-Node Shell Element for General Nonlinear Analysis," Engineering Computations, VI, No. 1, pp. 77-88.

W. Flügge (1973), Stresses in Shells, 2nd Edition, Springer-Verlag, Berlin.

I. Fried (1973), "Shape Functions and the Accuracy of Arch Finite Elements," AIAA J., 11, p. 287.

T.J.R. Hughes, R.L. Taylor and W. Kanoknukulchai (1977), "A Simple and Efficient Element for Plate Bending," Int. J. Num. Meth. Eng., 10, 11, pp. 1529-1543.

T.J.R. Hughes and W.K. Liu (1981), "Nonlinear Finite element Analysis of Shells: Part I. Three Dimensional Shells," Comp. Meth. Appl. Mech. Eng., 26, pp. 331-362.

T.J.R. Hughes and T.E. Tezduyar (1981), "Finite Elements Based Upon Mindlin Plate Theory with Particular Reference to the Four-Node Isoparametric Element," J. Appl. Mech., 48, pp. 587-596.

S. Idelsohn (1981), "On the Use of Deep Shallow or Flat Shell Elements for the Analysis of Thin Shell Structures," Computer Methods in Applied Mechanics and Eng. 26, pp. 321-330.

F. Kikuchi (1982), "Accuracy of Some Finite Element Models for Arch Problems," Comp. Meth. Appl. Mech. Eng., 35, pp. 315-345.

F. Kikuchi and T. Aizawa (1982), "Locking Phenomena in Finite Element Analysis of Large Deflection Problems," Proc. of the 32nd Japan National Congress for Applied Mechanics, University of Tokyo Press.
S.W. Lee and T.H.H. Pian (1978), "Improvement of Plate and Shell Finite Elements by Mixed Formulations," AIAA Journal, 1, 16, pp. 29-34.

G.M. Lindberg, M.D. Olson and G.R. Cowper (1969), "New Developments in the Finite Element Analysis of Shells," Q. Bull. Div. Mech. Eng. and the National Aeronautical Establishment, National Research Council of Canada, Vol. 4.

W.K. Liu, T. Belytschko, S.E. Law and D. Lam (1985), "Resultant Stress Degenerated Shell Element," submitted to Comp. Meth. in Appl. Mech. and Eng.

R.H. MacNeal (1982), "Derivation of Element Stiffness Matrices by Assumed Strain Distribution," Nucl. Eng. and Design, 70, pp. 3-12.

R.H. MacNeal and R.L. Harder (1984), "A Proposed Standard Set of Problems to Test Finite Element Accuracy," Proc. of AIAA Conf. on Structures and Structural Dynamics, Palm Springs, California.

D.S. Malkus and T.J.R. Hughes (1978), "Mixed Finite Element Methods - Reduced and Selective Integration Techniques: A Unification of Concepts," Comp. Meth. Appl. Mech. Engrg., 15, pp. 63-81.

L.S.D. Morley (1972), "Polynomial Stress States in first Approximation Theory of Circular Cylindrical Shells," Quart. J. Mech. and Appl. Math., 25, p. 13.

L.S.D. Morley and A.J. Morris (1978), "Conflict Between Finite Elements and Shell Theory," Royal Aircraft Establishment Report, London.

L.S.D. Morley (1983), "Quality of Trial Functions in Quadratic Isoparametric Representation of an Arc," Int. J. Num. Meth. Eng., 1, 19, pp. 37-48.

A.K. Noor and J.M. Peters (1981), "Mixed Models and Reduced/Selective Integration Displacement Models for Nonlinear Analysis of Curved Beams," Int. J. Num. Meth. Eng., 17, pp. 615-631.

J.T. Oden and J.N. Reddy (1974), "On Dual-Complementary Variational Principles in Mathematical Physics," Int. J. Eng. Science, 12, pp. 1-29.

M.D. Olson and T.W. Bearden (1979), "A Simple Flat Triangular Shell Element Revisited," Int. J. Num. Meth. Eng., 14, pp. 51-68.

H. Parish (1979), "A Critical Survey of the 9-Node Degenerated Shell Element with Special Emphasis on Thin Shell Application and Reduced Integration," Comp. Meth. Appl. Mech. & Eng., 20, pp. 323-350.

K.C. Park and D.L. Flaggs, "A Fourier Analysis of Spurious Mechanisms and Locking in Computational Mechanics," Comp. Meth. Appl. Mech. Eng., to appear.

G. Prathap and G.R. Bhashyam (1982), "Reduced Integration and the Shear-Flexible Beam Element," Int. J. Num. Meth. Eng., 18, pp. 195-210.

E. Ramm and H. Stegmüller (1982), "The Displacement Finite Element Method in Nonlinear Buckling Analysis of Shells," in Buckling of Shells, (Ed. by E. Ramm), Springer-Verlag, Berlin, pp. 201-235.

A.B. Sabir and D.G. Ashwell (1971), "A Comparison of Curved Beam Finite Elements When Used in Vibration Problems," J. Sound Vib., 18, p. 555.

A.B. Sabir and A.C. Lock (1973), "Large Deflection, Geometrically Nonlinear Analysis of Circular Arches," Int. J. Mech. Sci. 15, pp. 37-47.

A.C. Scordelis and K.S. Lo (1969), "Computer Analysis of Cylindrical Shells," J. Am. Concr. Inst., 61, pp. 539-561.

H. Stolarski and T. Belytschko (1981), "Reduced Integration for Shallow-Shell Facet Elements," in New Concepts in Finite Element Analysis, (Ed. by T.J.R. Hughes, D. Gartling and R.L. Spilker) published by ASME.

H. Stolarski and T. Belytschko (1982), "Membrane Locking and Reduced Integration for Curved Elements," J. Appl. Mech., 49, pp. 172-176.

H. Stolarski and T. Belytschko (1983), "Shear and Membrane Locking in Curved C^0 Elements," Comp. Meth. Appl. Mech. Eng., 41, pp. 279-296.

H. Stolarski, T. Belytschko, N. Carpenter and J.M. Kennedy (1984a), "A Simple Triangular Curved Shell Element for Collapse Analysis," in Collapse Analysis of Structures," (Ed. by L.H. Sobel and K. Thomas), published by ASME.

H. Stolarski, T. Belytschko, N. Carpenter and J.M. Kennedy (1984b), "A Simple Triangular Curved Shell Element," Engineering Computations, to appear.

H. Stolarski and T. Belytschko (1985a), "On the Equivalence of Mode Decomposition and Mixed Finite Elements," submitted to Comp. Meth. Appl. Mech. Eng..

H. Stolarski, N. Carpenter and T. Belytschko (1985b), "Some Aspects of Finite Element Analysis of Shells," in preparation.

G. Wempner, D. Talaslidis and C.-M. Hwang (1982), "A Simple and Efficient Approximation of Shells via Finite Quadrilateral Elements," J. Appl. Mech., 1, 49, pp. 115-120.

O.C. Zienkiewicz, R.L. Taylor and J.M. Too (1971), "Reduced Integration Technique in General Analysis of Plates and Shells," Int. J. Num. Meth. Eng., 3, pp. 275-290.

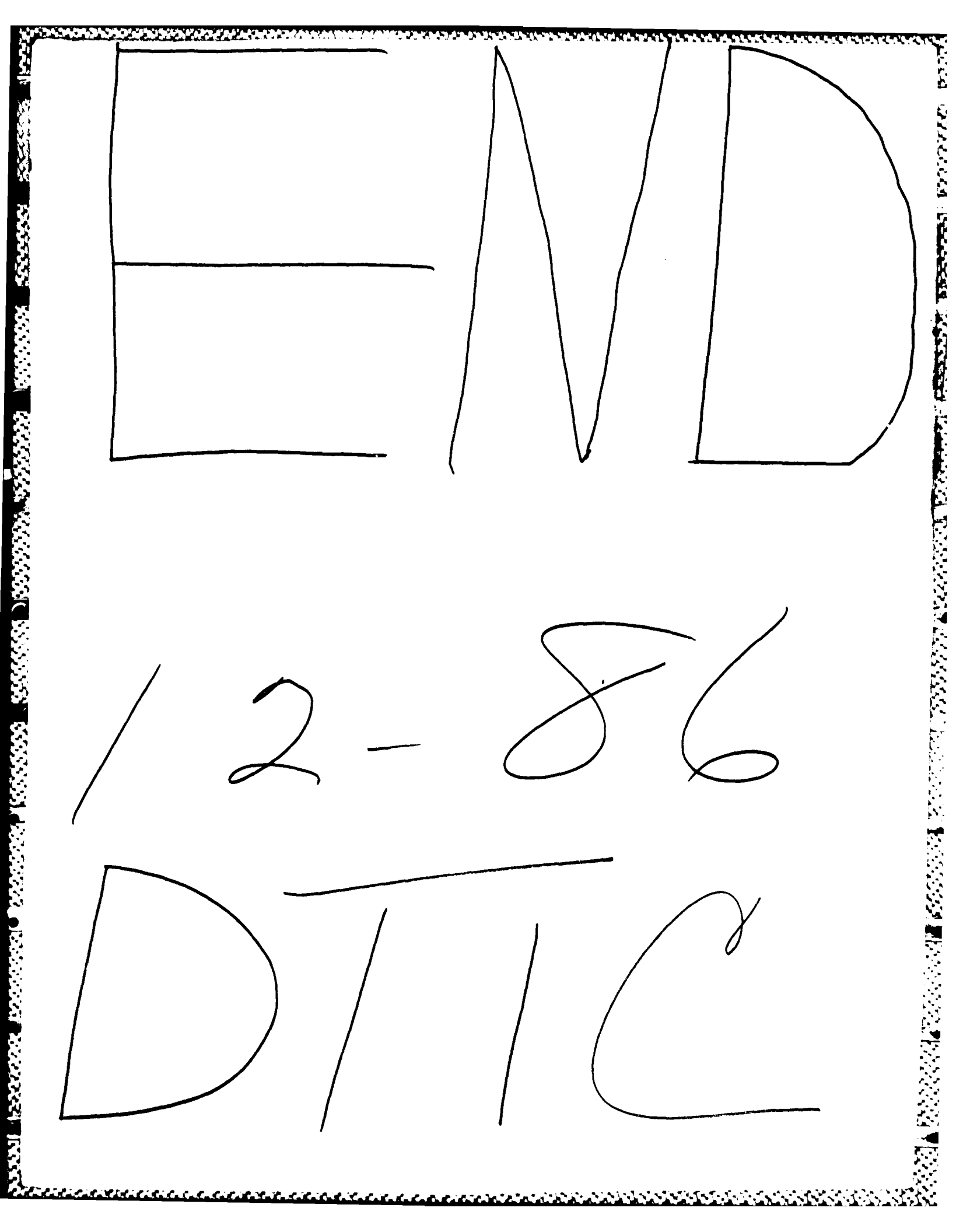
END
12-86
DTIC